Abstracta

Ano XXIII - N. 03

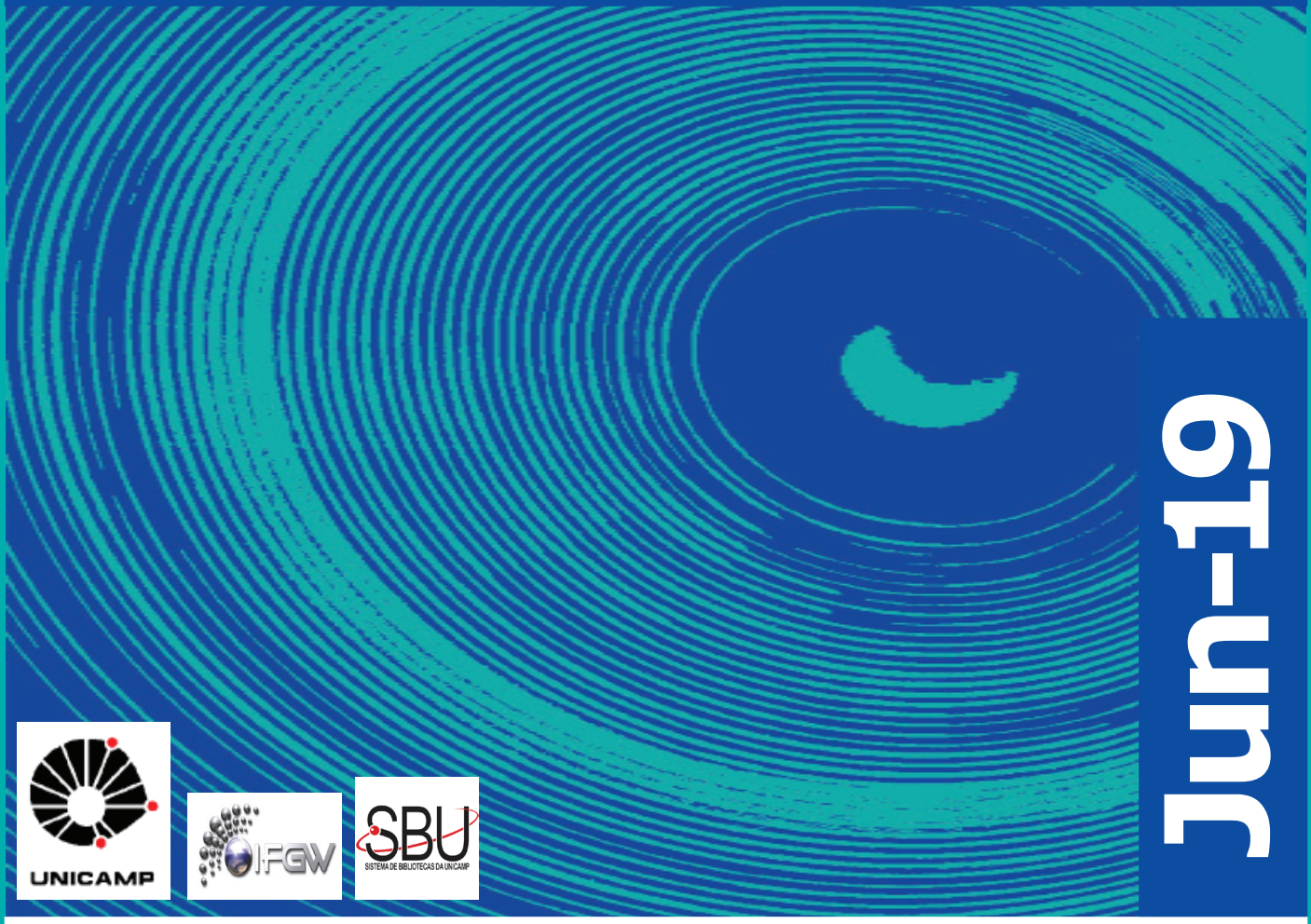

Jun-19

Artigos publicados - P142-2019 à P231-2019

Correções - Co001-2019

Defesas de Teses do IFGW - T006-2019

Defesas de Dissertações do IFGW - D005-2019 à D014-2019

Artigos publicados

[P142-2019] "A Search for Optical Emission from Binary Black Hole Merger GW170814 with the Dark Energy Camera"

Doctor, Z.; Kessler, R.; Herner, K.; **Sobreira, F.***; et. al.; DES Collaboration

Binary black hole (BBH) mergers found by the Laser Interferometer Gravitational-Wave Observatory (LIGO) and Virgo detectors are of immense scientific interest to the astrophysics community, but are considered unlikely to be sources of electromagnetic emission. To test whether they have rapidly fading optical counterparts, we used the Dark Energy Camera to perform an i-band search for the BBH merger GW170814, the first gravitational wave (GW) detected by three interferometers. The 87 deg(2) localization region (at 90% confidence) centered in the Dark Energy Survey (DES) footprint enabled us to image 86% of the probable sky area to a depth of i similar to 23 mag and provide the most comprehensive data set to search for electromagnetic (EM) emission from BBH mergers. To identify candidates, we perform difference imaging with our search images and with templates from pre-existing Dark Energy Survey (DES) images. The analysis strategy and selection requirements were designed to remove supernovae and to identify transients that decline in the first two epochs. We find two candidates, each of which is spatially coincident with a star or a high-redshift galaxy in the DES catalogs, and they are thus unlikely to be associated with GW170814. Our search finds no candidates associated with GW170814, disfavoring rapidly declining optical emission from BBH mergers brighter than i similar to 23 mag (L-optical similar to 5 x 10(41) erg s(-1)) 1-2 days after coalescence. In terms of GW sky map coverage, this is the most complete search for optical counterparts to BBH mergers to date.

ASTROPHYSICAL JOURNAL LETTERS [873], 2, L24, 2019. DOI: 10.3847/2041-8213/ab08a3

[P143-2019] "Acceleration of the precession frequency for optically-oriented electron spins in ferromagnetic/semiconductor hybrids"

Moraes, F. C. D.; Ullah, S.; **Balanta, M. A. G.*; Iikawa, F.***; Danilov, Y. A.; Dorokhin, M., V; Vikhrova, O. V.; Zvonkov, B. N.; Hernandez, F. G. G.

Time-resolved Kerr rotation measurements were performed in InGaAs/GaAs quantum wells nearby a doped Mn delta layer. Our magneto-optical results show a typical time evolution of the optically oriented electron spin in the quantum well. Surprisingly, this is strongly affected by the Mn spins, resulting in an increase of the spin precession frequency in time. This increase is attributed to the variation in the effective magnetic field induced by the dynamical relaxation of the Mn spins. Two processes are observed during electron spin precession: a quasi-instantaneous alignment of the Mn spins with photo-excited holes, followed by a slow alignment of Mn spins with the external transverse magnetic field. The first process leads to an equilibrium state imprinted in the initial precession frequency, which depends on pump power, while the second process promotes a linear frequency increase, with acceleration depending on temperature and external magnetic field. This observation yields new information about exchange process dynamics and on the possibility of constructing spin memories, which can rapidly respond to light while retaining information for a longer period.

SCIENTIFIC REPORTS [9], 7294, 2019. DOI: 10.1038/s41598-019-43741-2

[P144-2019] "Acoustically modulated optical emission of hexagonal boron nitride layers"

Iikawa, F.*; Hernandez-Minguez, A.; Aharonovich, I.; Nakhaie, S.; Liou, Yi-Ting; Lopes, J. M. J.; Santos, P. V

We investigate the effect of surface acoustic waves on the atomic-like optical emission from defect centers in hexagonal boron nitride layers deposited on the surface of a LiNbO3 substrate. The dynamic strain field of the surface acoustic waves modulates the emission lines resulting in intensity variations as large as 50% and oscillations of the emission energy with an amplitude of almost 1 meV. From a systematic study of the dependence of the modulation on the acoustic wave power, we determine a hydrostatic deformation potential of about 40 meV/% for defect centers in this two-dimensional material. Furthermore, we show that the dynamic piezoelectric field of the acoustic wave could contribute to the stabilization of the optical properties of these emission centers. Our results show that surface acoustic waves are a powerful tool to modulate and control the electronic states of two-dimensional materials.

APPLIED PHYSICS LETTERS [114], 17, 171104, 2019. DOI: 10.1063/1.5093299

[P145-2019] "Analysis of structural distortion in Eshelby twisted InP nanowires by scanning precession electron diffraction"

Ugarte, D.*; Tizei, L. H. G.; **Cotta, M. A.***; Ducati, C.; Midgley, P. A.; Eggeman, A. S.

Transmission electron microscopes (TEM) are widely used in nanotechnology research. However, it is still challenging to characterize nanoscale objects; their small size coupled with dynamical diffraction makes interpreting real- or reciprocal-space data difficult. Scanning precession electron diffraction ((S)PED) represents an invaluable contribution, reducing the dynamical contributions to the diffraction pattern at high spatial resolution. Here a detailed analysis of wurtzite InP nanowires (30-40 nm in diameter) containing a screw dislocation and an associated wire lattice torsion is presented. It has been possible to characterize the dislocation with great detail (Burgers and line vector, handedness). Through careful measurement of the strain field and comparison with dynamical electron diffraction simulations, this was found to be compatible with a Burgers vector modulus equal to one hexagonal lattice cell parameter despite the observed crystal rotation rate being larger (ca. 20%) than that predicted by classical elastic theory for the nominal wire diameter. These findings corroborate the importance of the (S)PED technique for characterizing nanoscale materials.

NANO RESEARCH [12], 4, 939-946, 2019. DOI: 10.1007/s12274-019-2328-5

[P146-2019] "Anisotropic magnetic excitations and incipient Neel order in Ba(Fe1-xMnx)(2)As-2"

Garcia, F. A.; Ivashko, O.; McNally, D. E.; Das, L.; **Piva, M. M.*; Adriano, C.*; Pagliuso, P. G.***; Chang, J.; Schmitt, T.; Monney, C.

It is currently understood that high temperature superconductivity (SC) in the transition metal (M) substituted iron arsenides Ba(Fe1-xMx)(2)As-2 is promoted by magnetic excitations with wave vectors (pi, 0) or (0, pi). It is known that while a small amount of Co substitution lead to SC, the same does not occur for Mn for any value of x. In this work, magnetic excitations in the iron arsenides Ba(Fe1-xMnx)(2)As-2 (x = 0.0, 0.007, 0.009, 0.08) are investigated by means of resonant inelastic x-ray scattering (RIXS) at the Fe L-3 edge, for momentum transfer q along the high symmetry Brillouin zone (pi, 0) and (pi, pi) directions. It is shown that with increasing Mn content (x), the excitations become anisotropic both in dispersion and lineshape. Both effects are detected even for small values of x, evidencing a cooperative phenomenon between the Mn impurities,

that we ascribe to emerging Neel order of the Mn spins. Moreover, for x = 0.08, the excitations along q parallel to (pi, 0) are strongly damped and nearly nondispersive. This result suggests that phases of arsenides containing local moments at the FeAs layers, as in Mn or Cr substituted phases, do not support high temperature SC due to the absence of the appropriate magnetic excitations.

PHYSICAL REVIEW B [99], 11, 115118, 2019. DOI: 10.1103/PhysRevB.99.115118

[P147-2019] "Atomically locked interfaces of metal (Aluminum) and polymer (Polypropylene) using mechanical friction"

Rout, A.; Pandey, P.; **Oliveira, E. F.*; Autreto, P. A. S.***; Gumaste, A.; Singh, A.; **Galvao, D. S.***; Arora, A.; Tiwary, C. S.

Joining different parts is one of the crucial components of designing/engineering of materials. Presently, the current energy efficient low weight automotive and aerospace components consist of a different class of materials, such as metals, polymers, ceramics, etc. Joining these components remains a challenge. Here, we demonstrate metal (aluminum) and polymer (Polypropylene, pp) joining using mechanical friction. The detailed characterization clearly demonstrates that atomically locked interfaces are formed in such joining and no chemical bonds are formed during the joining. Also, a waterproof and strong interface is formed in such a process. Fully atomistic molecular dynamics simulations were also carried out in order to further gain insights on the joining process.

POLYMER [169], SI, 148-153, 2019. DOI: 10.1016/j.polymer.2019.02.049

[P148-2019] "Candidate massive galaxies at z similar to 4 in the Dark Energy Survey"

Guarnieri, P.; Maraston, C.; Thomas, D.; **Sobreira, F..***; et. al.

Using stellar population models, we predicted that the Dark Energy Survey (DES) - due to its special combination of area (5000 deg(2)) and depth (i = 24.3) - would be in the position to detect massive (greater than or similar to 10(11) M-circle dot) galaxies at z similar to 4. We confront those theoretical calculations with the first similar to 150 deg(2) of DES data reaching nominal depth. From a catalogue containing similar to 5 million sources, similar to 26 000 were found to have observed--frame g - r versus r - i colours within the locus predicted for z similar to 4 massive galaxies. We further removed contamination by stars and artefacts, obtaining 606 galaxies lining up by the model selection box. We obtained their photometric redshifts and physical properties by fitting model templates spanning a wide range of star formation histories, reddening and redshift. Key to constrain the models is the addition, to the optical DES bands g, r, i, z, and Y, of near-IR J, H, K-s data from the Vista Hemisphere Survey. We further applied several quality cuts to the fitting results, including goodness of fit and a unimodal redshift probability distribution. We finally select 233 candidates whose photometric redshift probability distribution function peaks around z similar to 4, have high stellar masses [log (M*/M-circle dot) similar to 11.7 for a Salpeter IMF] and ages around 0.1 Gyr, i.e. formation redshift around 5. These propertiesmatch those of the progenitors of the most massive galaxies in the local Universe. This is an ideal sample for spectroscopic follow-up to select the fraction of galaxies which are truly at high redshift. These initial results and those at the survey completion, which we shall push to higher redshifts, will set unprecedented constraints on galaxy formation, evolution, and the re-ionization epoch.

MONTHLY NOTICES OF THE ROYAL ASTRONOMICAL SOCIETY [483], 3, 3060-3081, 2019. DOI: 10.1093/mnras/sty3305

[P149-2019] "Charged-particle pseudorapidity density at mid-rapidity in p-Pb collisions at root S-NN=8.16 TeV"

Acharya, S.; Acosta, F. T.; Adamova, D.; **Albuquerque, D. S. D.*; Chinellato, D. D.*; De Souza, R. D.*; Takahashi, J.***; et. al.; ALICE Collaboration

The pseudorapidity density of charged particles, dN(ch)/d eta, in p-Pb collisions has been measured at a centre of-mass energy per nucleon-nucleon pair of root S-NN = 8.16 TeV at mid--pseudorapidity for non-single-diffractive events. The results cover 3.6 units of pseudorapidity, vertical bar eta vertical bar < 1.8. The dN(ch)/d eta value is 19.1 +/- 0.7 at vertical bar eta vertical bar < 0.5. This quantity divided by < N-part >/2 is 4.73 +/- 0.20, where < N-part > is the average number of participating nucleons, is 9.5% higher than the corresponding value for p-Pb collisions at root S-NN = 5.02 TeV. Measurements are compared with models based on different mechanisms for particle production. All models agree within uncertainties with data in the Pb-going side, while HIJING overestimates, showing a symmetric behaviour, and EPOS underestimates the p-going side of the dN(ch)/d eta distribution. Saturation--based models reproduce the distributions well for eta > -1.3. The dN(ch)/d eta is also measured for different centrality estimators, based both on the charged particle multiplicity and on the energy deposited in the Zero Degree Calorimeters. A study of the implications of the large multiplicity fluctuations due to the small number of participants for systems like p-Pb in the centrality calculation for multiplicity-based estimators is discussed, demonstrating the advantages of determining the centrality with energy deposited near beam rapidity.

EUROPEAN PHYSICAL JOURNAL C [79], 4, 307, 2019. DOI: 10.1140/epjc/s10052-019-6801-9

[P150-2019] "Combination of Searches for Higgs Boson Pair Production in Proton-Proton Collisions at root s=13 TeV"

Sirunyan, A. M.; Tumasyan, A.; Adam, W.; **Chinellato, J. A.*; Tonelli Manganote, E. J.***; et. al.; CMS Collaboration

This Letter describes a search for Higgs boson pair production using the combined results from four final states: bb gamma gamma, bb tau tau, bbbb, and bbVV, where V represents a W or Z boson. The search is performed using data collected in 2016 by the CMS experiment from LHC proton-proton collisions at root s = 13 TeV, corresponding to an integrated luminosity of 35.9 fb(-1). Limits are set on the Higgs boson pair production cross section. A 95% confidence level observed (expected) upper limit on the non-resonant production cross section is set at 22.2 (12.8) times the standard model value. A search for narrow resonances decaying to Higgs boson pairs is also performed in the mass range 250-3000 GeV. No evidence for a signal is observed, and upper limits are set on the resonance production cross section.

PHYSICAL REVIEW LETTERS [122], 12, 121803, 2019. DOI: 10.1103/PhysRevLett.122.121803

[P151-2019] "Computational approach to determine the relative biological effectiveness of fast neutrons using the Geant4-DNA toolkit and a DNA atomic model from the Protein Data Bank"

Zabihi, A.; Incerti, S.; Francis, Z.; Forozani, G.; Semsarha, F.; Moslehi, A.; Rezaeian, P.; **Bernal, M. A.***

This study proposes an innovative approach to estimate relative biological effectiveness (RBE) of fast neutrons using the Geant4 toolkit. The Geant4-DNA version cannot track heavy ions below 0.5 MeV/nucleon. In order to explore the impact of this issue, secondary particles are simulated instead of the primary low-energy neutrons.

The Evaluated Nuclear Data File library is used to determine the cross sections for the elastic and inelastic interactions of neutrons with water and to find the contribution of each secondary particle spectrum. Two strategies are investigated in order to find the best possible approach and results. The first one takes into account only light particles, protons produced from elastic scattering, and a particles from inelastic scattering. Geantino particles are shot instead of heavy ions; hence all heavy ions are considered in the simulations, though their physical effects on DNA not. The second strategy takes into account all the heavy and light ions, although heavy ions cannot be tracked down to very low energies (E < 0.5 MeV/nucleon). Our model is based on the combination of an atomic resolution DNA geometrical model and a Monte Carlo simulation toolkit for tracking particles. The atomic coordinates of the DNA double helix are extracted from the Protein Data Bank. Since secondary particle spectra are used instead of simulating the interaction of neutrons explicitly, this method reduces the computation times dramatically. Double-strand break induction is used as the end point for the estimation of the RBE of fast neutrons. Co-60 gamma rays are used as the reference radiation quality. Both strategies succeed in reproducing the behavior of the RBEmax as a function of the incident neutron energy ranging from 0.1 to 14 MeV, including the position of its peak. A comparison of the behavior of the two strategies shows that for neutrons with energies less than 0.7 MeV, the effect of heavy ions would not be very significant, but above 0.7 MeV, heavy ions have an important role in neutron RBE.

PHYSICAL REVIEW E [99], 5, 052404, 2019. DOI: 10.1103/PhysRevE.99.052404

[P152-2019] "Connecting Theory with Experiment to Understand the Sintering Processes of Ag Nanoparticles"

Silva, E. Z.*; Faccin, G. M.; Machado, T. R.; Macedo, N. G.; de Assis, M.; Maya-Johnson, S.; Sczancoski, J. C.; Andres, J.; Longo, E.; San-Miguel, M. A.

A complementary combination of long-time atomistic molecular dynamics simulations and real-time transmission electron microscopy (TEM) images has been utilized for unraveling, at an atomic resolution, the nature of the sintering process of Ag nanoparticles (NPs) induced on the surface of an alpha-Ag2WO4 crystal for the first time, under the exposure of a TEM electron beam (EB). Temporal evolution of calculated and experimental results highlights the role of the lattice plane matching and the stacking faults along the disorder-to-order transitions of the oriented attachment process. This phenomenon is considered as an example of surface plasmon resonances (SPRs), in which the EB has two effects: first, it provokes the formation of the Ag NPs that, due to the electron irradiation, become SPR electric dipoles, and, second, these Ag NPs undergo sintering processes that are controlled by dipole-dipole interactions forming larger clusters. The predictive power of the simulation model was verified experimentally, paving the way for quantitative predictions of the events involved in the Ag NP sintering process. These findings reveal the atomic-scale dynamics, which helps advance the general understanding and provides further support and reliability of the conclusions of this study.

JOURNAL OF PHYSICAL CHEMISTRY C [123], 17, 11310-11318, 2019. DOI: 10.1021/acs.jpcc.9b02107

[P153-2019] "Constraints on axionic dark matter in the 3-3-1 model"

Castellanos, A. R.*; Alvarez-Salazar, C. E.*; Sanchez-Vega, B. L.

Dark matter in the form of axions can be included in models with SU(3)(C) circle times SU(3)(L) circle times U(1)(X) symmetry with right-handed neutrinos, where the strong charge-parity (CP) problem can be solved. Different versions of the model have the appealing characteristic of giving the observed dark matter abundance, measured by the Planck collaboration, for suitable values of the parameters. We studied the constraints on the parameter space of the model obtained when the axion mass is calculated taking into account both quantum chromodynamics (QCD) effects and gravitationally induced operators, making a comparison of three different models.

ASTRONOMISCHE NACHRICHTEN, 340, 1-3, SI, 131-134, 2019. DOI: 10.1002/asna.201913576

[P154-2019] "Cosmological Constraints from Multiple Probes in the Dark Energy Survey"

Abbott, T. M. C.; Alarcon, A.; Allam, S.; **Sobreira, F.***; et. al.; DES Collaboration

The combination of multiple observational probes has long been advocated as a powerful technique to constrain cosmological parameters, in particular dark energy. The Dark Energy Survey has measured 207 spectroscopically confirmed type Ia supernova light curves, the baryon acoustic oscillation feature, weak gravitational lensing, and galaxy clustering. Here we present combined results from these probes, deriving constraints on the equation of state, w, of dark energy and its energy density in the Universe. Independently of other experiments, such as those that measure the cosmic microwave background, the probes from this single photometric survey rule out a Universe with no dark energy, finding w = -0.80(-0.11)(+0.09). The geometry is shown to be consistent with a spatially flat Universe, and we obtain a constraint on the baryon density of Omega(b) = 0.069(-0.012)(+0.009) that is independent of early Universe measurements. These results demonstrate the potential power of large multiprobe photometric surveys and pave the way for order of magnitude advances in our constraints on properties of dark energy and cosmology over the next decade.

PHYSICAL REVIEW LETTERS [122], 17, 171301, 2019. DOI: 10.1103/PhysRevLett.122.171301

[P155-2019] "Cranial and endocranial diversity in extant and fossil atelids (Platyrrhini: Atelidae): A geometric morphometric study"

Aristide, L.; Strauss, A.; Halenar-Price, L. B.; Gilissen, E.; Cruz, F. W.; Cartelle, C.; Rosenberger, A. L.; Lopes, R. T.; dos Reis, S. F.; **Perez, S. I.***

Objectives Platyrrhines constitute a diverse clade, with the modern Atelidae exhibiting the most variation in cranial and endocast morphology. The processes responsible for this diversification are not well understood. Here, we present a geometric morphometric study describing variation in cranial and endocranial shape of 14 species of Alouatta, Ateles, Brachyteles, and Lagothrix and two extinct taxa, Cartelles and Caipora. Methods We examined cranial and endocranial shape variation among species using images reconstructed from CT scans and geometric morphometric techniques based on three-dimensional landmarks and semilandmarks. Principal components analyses were used to explore variation, including the Procrustes shape coordinates, summing the logarithm of the Centroid Size, the common allometric component, and residual shape components. Results Differences in endocranial shape are related to a relative increase or decrease in the volume of the neocortex region with respect to brainstem and cerebellum regions. The relative position of the brainstem varies from a posterior position in Alouatta to a more ventral position in Ateles.

The shape of both the cranium and endocast of Caipora is within the observed variation of Brachyteles. Cartelles occupies the most differentiated position relative to the extant taxa, especially in regards to its endocranial shape. Conclusions The pattern of variation in the extant species in endocranial shape is similar to the variation observed in previous cranial studies, with Alouatta as an outlier. The similarities between Caipora and Brachyteles were unexpected and intriguing given the frugivorous adaptations inferred from the fossil's dentition. Our study shows the importance of considering both extant and fossil species when studying diversification of complex traits.

AMERICAN JOURNAL OF PHYSICAL ANTHROPOLOGY [169], 2, 322-331, 2019. DOI: 10.1002/ajpa.23837

[P156-2019] "Dark Energy Survey Year 1 Results: Detection of Intracluster Light at Redshift similar to 0.25"

Zhang, Y.; Yanny, B.; Palmese, A.; **Sobreira, F.***; et. al.; DES Collaboration

Using data collected by the Dark Energy Survey (DES), we report the detection of intracluster light (ICL) with similar to 300 galaxy clusters in the redshift range of 0.2-0.3. We design methods to mask detected galaxies and stars in the images and stack the cluster light profiles, while accounting for several systematic effects (sky subtraction, instrumental point--spread function, cluster selection effects, and residual light in the ICL raw detection from background and cluster galaxies). The methods allow us to acquire high signal-to-noise measurements of the ICL and central galaxies (CGs), which we separate with radial cuts. The ICL appears as faint and diffuse light extending to at least 1 Mpc from the cluster center, reaching a surface brightness level of 30 mag arcsec(-2). The ICL and the cluster CG contribute 44% +/- 17% of the total cluster stellar luminosity within 1 Mpc. The ICL color is overall consistent with that of the cluster red sequence galaxies, but displays the trend of becoming bluer with increasing radius. The ICL demonstrates an interesting self-similarity feature-for clusters in different richness ranges, their ICL radial profiles are similar after scaling with cluster R-200(m), and the ICL brightness appears to be a good tracer of the cluster radial mass distribution. These analyses are based on the DES redMaPPer cluster sample identified in the first year of observations.

ASTROPHYSICAL JOURNAL [874], 2, 165, 2019. DOI: 10.3847/1538-4357/ab0dfd

[P157-2019] "Dark Energy Survey Year 1 results: measurement of the baryon acoustic oscillation scale in the distribution of galaxies to redshift 1"

Abbott, T. M. C.; Abdalla, F. B.; Alarcon, A.; **Sobreira, F.***; et. al.; Dark Energy Survey Collaboration

We present angular diameter distance measurements obtained by locating the baryon acoustic oscillations (BAO) scale in the distribution of galaxies selected from the first year of Dark Energy Survey data. We consider a sample of over 1.3 million galaxies distributed over a footprint of 1336 deg(2) with 0.6 < z(photo) < 1 and a typical redshift uncertainty of 0.03(1 + z). This sample was selected, as fully described in a companion paper, using a colour/magnitude selection that optimizes trade-offs between number density and redshift uncertainty. We investigate the BAO signal in the projected clustering using three conventions, the angular separation, the comoving transverse separation, and spherical harmonics. Further, we compare results obtained from template-based and machine-learning photometric redshift determinations. We use 1800 simulations that approximate our sample in order to produce covariance matrices and allow us to validate our distance scale measurement methodology. We measure the angular diameter distance, D-A, at the effective redshift of our sample divided by the true physical scale of the BAO feature, r(d). We obtain close to a 4 per cent distance measurement of D-A (z(eff)= 0.81)/r(d) = 10.75 +/- 0.43. These results are consistent with the flat A cold dark matter concordance cosmological model supported by numerous other recent experimental results.

MONTHLY NOTICES OF THE ROYAL ASTRONOMICAL SOCIETY [483], 4, 4866-4883, 2019. DOI: 10.1093/mnras/sty3351

[P158-2019] "Electrochemical water oxidation by cobalt--Prussian blue coordination polymer and theoretical studies of the electronic structure of the active species"

Pires, B. M.; dos Santos, P. L.; Katic, V.; Strohauer, S.; **Landers, R.***; Formiga, A. L. B.; Bonacin, J. A.

The search for earth-abundant metal-based catalysts for the oxygen evolution reaction (OER) that operates under neutral conditions is a challenge in the field of sustainable energy. Many strategies have been used, and coordination polymers with structures similar to Prussian blue appear to be interesting electrocatalysts due to their efficiency, stability and tunable properties. In this paper, a novel catalyst produced from a cobalt-pentacyanidoferrate precursor is presented and applied in studies of the OER. This material showed a high surface active area and electrocatalytic activity comparable to traditional cobalt hexacyanidoferrate. According to the theoretical calculations, the improvement of these properties is an effect of the framework arrangement and it is not caused by changes of the electronic structure. Further experimental evidence is necessary to determine the active species. However, our results of spin densities obtained from DFT calculations suggest that the active species for water oxidation is the radical Fe(III)CN-Co(III)-O-center dot.

DALTON TRANSACTIONS [48], 15, 4811-4822, 2019. DOI: 10.1039/c8dt04660c

[P159-2019] "Electronic structure of Fe and magnetism in the 3d/5d double perovskites Ca2FeReO6 and Ba2FeReO6"

Granado, E.*; Cezar, J. C.; **Azimonte, C.***; Gopalakrishnan, J.; Ramesha, K.

The Fe electronic structure and magnetism in (i) monoclinic Ca2FeReO6 with a metal-insulator transition at T-MI similar to 140 K and (ii) quasicubic half-metallic Ba2FeReO6 ceramic double perovskites are probed by soft x-ray absorption spectroscopy (XAS) and magnetic circular dichroism (XMCD). These materials show distinct Fe L-2,L-3 XAS and XMCD spectra, which are primarily associated with their different average Fe oxidation states (close to Fe3+ for Ca2FeReO6 and intermediate between Fe2+ and Fe3+ for Ba2FeReO6) despite being related by an isoelectronic (Ca2+/Ba2+) substitution. For Ca2FeReO6, the powder-averaged Fe spin moment along the field direction (B = 5 T), as probed by the XMCD experiment, is strongly reduced in comparison with the spontaneous Fe moment previously obtained by neutron diffraction, consistent with a scenario where the magnetic moments are constrained to remain within an easy plane. For B = 1 T, the unsaturated XMCD signal is reduced below T-MI consistent with a magnetic transition to an easy-axis state that further reduces the powder-averaged magnetization in the field direction. For Ba2FeReO6, the field--aligned Fe spins are larger than for Ca2FeReO6 (B = 5 T) and the temperature dependence of the Fe magnetic moment is consistent with the magnetic ordering transition at T-C(Ba) = 305 K. Our results illustrate the dramatic influence of the specific spin-orbital configuration of Re 5d electrons on the Fe 3d local magnetism of these Fe/Re double perovskites.

PHYSICAL REVIEW B [99], 19, 195118, 2019. DOI: 10.1103/PhysRevB.99.195118

[P160-2019] "Energy dependence of exclusive J/ photoproduction off protons in ultra-peripheral p-Pb collisions at NN=5.02 TeV"

Acharya, S.; Acosta, F. T.; Adam, J.; **Albuquerque, D. S. D.*; Chinellato, D. D.*; De Souza, R. D.*; Takahashi, J.***; et. al.; ALICE Collaboration

The ALICE Collaboration has measured the energy dependence of exclusive photoproduction of J/ vector mesons off proton targets in ultra-peripheral p-Pb collisions at a centre--of-mass energy per nucleon pair =5.02 TeV. The e+e- and +- decay channels are used to measure the cross section as a function of the rapidity of the J/ in the range -2.5<y<2.7, corresponding to an energy in the p centre-of-mass in the interval 40<Wp<550 GeV. The measurements, which are consistent with a power law dependence of the exclusive J/ photoproduction cross section, are compared to previous results from HERA and the LHC and to several theoretical models. They are found to be compatible with previous measurements.

EUROPEAN PHYSICAL JOURNAL C [79], 5, 402, 2019. DOI: 10.1140/epjc/s10052-019-6816-2

[P161-2019] "Enhanced mobility and controlled transparency in multilayered reduced graphene oxide quantum dots: a charge transport study"

Jimenez, M. J. M.*; de Oliveira, R. F.; Bufon, C. C. B.; Pereira--da-Silva, M. A.; **Rodrigues, V.***; Gobbi, A. L.; Piazzetta, M. H. O.; **Alvarez, F.*; Cesar, C. L.*; Riul Jr, A.***

Reduced graphene oxide (rGO) layers are known to be significantly conductive along the basal plane throughout delocalized sp(2) domains Defects present in rGO implies in disordered systems with numerous localized sites, resulting in a charge transport governed mainly by a 2D variable range hopping (VRH) mechanism These characteristics are observed even in multilayered rGO since the through-plane conduction is expected to be insubstantial. Here, we report on the multilayer assembly of functionalized rGO quantum dots (GQDs) presenting 3D VRH transport that endows elevated charge carrier mobility, ca similar to 236 cm(2) V(-1)s(-1). Polyelectrolyte--wrapped GQDs were assembled by layer-by-layer technique (LbL), ensuring molecular level thickness control for the formed nanostructures, along with the adjustment of the film transparency (up to 92% in the visible region). The small size and the random distribution of GQDs in the LbL structure are believed to overcome the translational disorder in multilayered films, contributing to a 3D interlayer conduction that enhances the electronic properties. Such high-mobility, transparency--tunable films assembled by a cost-effective method possess interesting features and wide applicability in optoelectronics.

NANOTECHNOLOGY [30], 27, 275701, 2019, DOI: 10.1088/1361-6528/ab118e

[P162-2019] "Exploring Collagen Parameters in Pure Special Types of Invasive Breast Cancer"

Natal, R. A.; Paiva, G. R.; **Pelegati, V. B.*; Marenco, L.***; Alvarenga, C. A.; Vargas, R. F.; Derchain, S. F.; Sarian, L. O.; Franchet, C.; **Cesar, C. L.***; Schmitt, F. C.; Weigelt, B.; Vassallo, J.

One of the promising tools to evaluate collagen in the extracellular matrix is the second-harmonic generation microscopy (SHG). This approach may shed light on the biological behavior of cancers and their taxonomy, but has not yet been applied to characterize collagen fibers in cases diagnosed as invasive breast carcinoma (BC) of histological special types (IBC-ST). Tissue sections from 99 patients with IBC-ST and 21 of invasive breast carcinoma of no special type (IBC-NST) were submitted to evaluation of collagen parameters by SHG. Tissue microarray was performed to evaluate immunohistochemical-based molecular subtype. In intratumoral areas, fSHG and bSHG (forward-SHG and backward-SHG) collagen parameters achieved their lowest values in mucinous, papillary and medullary carcinomas, whereas the highest values were found in classic invasive lobular and tubular carcinomas. Unsupervised hierarchical cluster analysis and minimal spanning tree using intratumoral collagen parameters allowed the identification of three main groups of breast cancer: group A (classic invasive lobular and tubular carcinomas); group B (IBC-NST, metaplastic, invasive apocrine and micropapillary carcinomas); and group C (medullary, mucinous and papillary carcinomas). Our findings provide further characterization of the tumor microenvironment of IBC--ST. This understanding may add information to build more consistent tumor categorization and to refine prognostication.

SCIENTIFIC REPORTS [9], 7715, 2019. DOI: 10.1038/s41598-019-44156-9

[P163-2019] "Finding high-redshift strong lenses in DES using convolutional neural networks"

Jacobs, C.; Collett, T.; Glazebrook, K.; **Sobreira, F.***; et. al.; DES Collaboration

We search Dark Energy Survey (DES) Year 3 imaging data for galaxy-galaxy strong gravitational lenses using convolutional neural networks. We generate 250 000 simulated lenses at redshifts > 0.8 from which we create a data set for training the neural networks with realistic seeing, sky and shot noise. Using the simulations as a guide, we build a catalogue of 1.1 million DES sources with 1.8 < g - i < 5, 0.6 < g - r < 3, r_mag > 19, g_mag > 20, and i_mag > 18.2. We train two ensembles of neural networks on training sets consisting of simulated lenses, simulated non-lenses, and real sources. We use the neural networks to score images of each of the sources in our catalogue with a value from 0 to 1, and select those with scores greater than a chosen threshold for visual inspection, resulting in a candidate set of 7301 galaxies. During visual inspection, we rate 84 as 'probably' or 'definitely' lenses. Four of these are previously known lenses or lens candidates. We inspect a further 9428 candidates with a different score threshold, and identify four new candidates. We present 84 new strong lens candidates, selected after a few hours of visual inspection by astronomers. This catalogue contains a comparable number of high-redshift lenses to that predicted by simulations. Based on simulations, we estimate our sample to contain most discoverable lenses in this imaging and at this redshift range.

MONTHLY NOTICES OF THE ROYAL ASTRONOMICAL SOCIETY [484], 4, 5330-5349, 2019. DOI: 10.1093/mnras/stz272

[P164-2019] "First Cosmology Results Using SNe Ia from the Dark Energy Survey: Analysis, Systematic Uncertainties, and Validation"

Brout, D.; Scolnic, D.; Kessler, R.; **Sobreira, F.***; et. al.; DES Collaboration

We present the analysis underpinning the measurement of cosmological parameters from 207 spectroscopically classified SNe Ia from the first 3 years of the Dark Energy Survey Supernova Program (DES-SN), spanning a redshift range of 0.017 < z < 0.849.

We combine the DES-SN sample with an external sample of 122 low-redshift (z < 0.1) SNe. Ia, resulting in a "DES-SN3YR" sample of 329 SNe Ia. Our cosmological analyses are blinded: after combining our DES-SN3YR distances with constraints from the Cosmic Microwave Background, our uncertainties in the measurement of the dark energy equation-of-state parameter, w, are 0.042. (stat) and 0.059 (stat+syst) at 68% confidence. We provide a detailed systematic uncertainty budget, which has nearly equal contributions from photometric calibration, astrophysical bias corrections, and instrumental bias corrections. We also include several new sources of systematic uncertainty. While our sample is less than one-third the size of the Pantheon sample, our constraints on w are only larger by 1.4x, showing the impact of the DES-SN. Ia light-curve quality. We find that the traditional stretch and color standardization parameters of the DES-SNe. Ia are in agreement with earlier SN. Ia samples such as Pan-STARRS1 and the Supernova Legacy Survey. However, we find smaller intrinsic scatter about the Hubble diagram (0.077 mag). Interestingly, we find no evidence for a Hubble residual step (0.007 +/- 0.018 mag) as a function of host-galaxy mass for the DES subset, in 2.4 sigma tension with previous measurements. We also present novel validation methods of our sample using simulated SNe. Ia inserted in DECam images and using large catalog--level simulations to test for biases in our analysis pipelines.

ASTROPHYSICAL JOURNAL [874], 2, 150, 2019. DOI: 10.3847/1538-4357/ab08a0

[P165-2019] "First cosmology results using Type Ia supernova from the Dark Energy Survey: simulations to correct supernova distance biases"

Kessler, R.; Brout, D.; D'Andrea, C. B.; **Sobreira, F.***; et. al.; DES Collaboration

We describe catalogue-level simulations of Type Ia supernova (SN Ia) light curves in the Dark Energy Survey Supernova Program (DES-SN) and in low-redshift samples from the Center for Astrophysics (CfA) and the Carnegie Supernova Project (CSP). These simulations are used to model biases from selection effects and light-curve analysis and to determine bias corrections for SN Ia distance moduli that are used to measure cosmological parameters. To generate realistic light curves, the simulation uses a detailed SN Ia model, incorporates information from observations (point spread function, sky noise, zero-point), and uses summary information (e.g. detection efficiency versus signal-to--noise ratio) based on 10 000 fake SN light curves whose fluxes were overlaid on images and processed with our analysis pipelines. The quality of the simulation is illustrated by predicting distributions observed in the data. Averaging within redshift bins, we find distance modulus biases up to 0.05 mag over the redshift ranges of the low-z and DES-SN samples. For individual events, particularly those with extreme red or blue colour, distance biases can reach 0.4 mag. Therefore, accurately determining bias corrections is critical for precision measurements of cosmological parameters. Files used to make these corrections are available at https://des.ncsa.illinois.edu/releases/sn.

MONTHLY NOTICES OF THE ROYAL ASTRONOMICAL SOCIETY [485], 1, 1171-1187, 2019. DOI: 10.1093/mnras/stz463

[P166-2019] "First Cosmology Results Using Type Ia Supernovae from the Dark Energy Survey: Photometric Pipeline and Light-curve Data Release"

Brout, D.; Sako, M.; Scolnic, D.; **Sobreira, F.***; et. al.; DES Collaboration

We present griz light curves of 251 SNe Ia from the first 3 years of the Dark Energy Survey Supernova Program's (DES-SN) spectroscopically classified sample. The photometric pipeline described in this paper produces the calibrated fluxes and associated uncertainties used in the cosmological parameter analysis by employing a scene modeling approach that simultaneously models a variable transient flux and temporally constant host galaxy. We inject artificial point sources onto DECam images to test the accuracy of our photometric method. Upon comparison of input and measured artificial supernova fluxes, we find that flux biases peak at 3 mmag. We require corrections to our photometric uncertainties as a function of host galaxy surface brightness at the transient location, similar to that seen by the DES Difference Imaging Pipeline used to discover transients. The public release of the light curves can be found at https://des.ncsa.illinois.edu/releases/sn.

ASTROPHYSICAL JOURNAL [874], 1, 106, 2019. DOI: 10.3847/1538-4357/ab06c1

[P167-2019] "First Measurement of the Hubble Constant from a Dark Standard Siren using the Dark Energy Survey Galaxies and the LIGO/Virgo Binary-Black-hole Merger GW170814"

Soares-Santos, M.; Palmese, A.; Hartley, W.; **Sobreira, F.***; et. al.; DES Collaboration; LIGO Sci Collaboration; Virgo Collaboration

We present a multi-messenger measurement of the Hubble constant H-0 using the binary-black-hole merger GW170814 as a standard siren, combined with a photometric redshift catalog from the Dark Energy Survey (DES). The luminosity distance is obtained from the gravitational wave signal detected by the Laser Interferometer Gravitational-Wave Observatory (LIGO)/Virgo Collaboration (LVC) on 2017 August 14, and the redshift information is provided by the DES Year 3 data. Black hole mergers such as GW170814 are expected to lack bright electromagnetic emission to uniquely identify their host galaxies and build an object-by-object Hubble diagram. However, they are suitable for a statistical measurement, provided that a galaxy catalog of adequate depth and redshift completion is available. Here we present the first Hubble parameter measurement using a black hole merger. Our analysis results in H-0 = 75(-32)(+40) km s(-1) Mpc(-1) , which is consistent with both SN Ia and cosmic microwave background measurements of the Hubble constant. The quoted 68% credible region comprises 60% of the uniform prior range [20, 140] km s(-1) Mpc(-1) , and it depends on the assumed prior range. If we take a broader prior of [10, 220] km s(-1) Mpc(-1) , we find H-0 = 78(-24)(+96) km s(-1) Mpc(-1) (57% of the prior range). Although a weak constraint on the Hubble constant from a single event is expected using the dark siren method, a multifold increase in the LVC event rate is anticipated in the coming years and combinations of many sirens will lead to improved constraints on H-0.

ASTROPHYSICAL JOURNAL LETTERS [876], 1, L7, 2019. DOI: 10.3847/2041-8213/ab14f1

[P168-2019] "Free-Surface Variational Principle for an Incompressible Fluid with Odd Viscosity"

Abanov, A. G.; **Monteiro, G. M.***

We present variational and Hamiltonian formulations of incompressible fluid dynamics with a free surface and nonvanishing odd viscosity. We show that within the variational principle the odd viscosity contribution corresponds to geometric boundary terms. These boundary terms modify Zakharov's Poisson brackets and lead to a new type of boundary dynamics. The modified boundary conditions have a natural geometric interpretation describing an additional pressure at the free surface proportional to the angular velocity of the surface itself. These boundary conditions are believed to be universal since the proposed hydrodynamic action is fully determined by the symmetries of the system.

PHYSICAL REVIEW LETTERS [122], 15, 154501, 2019. DOI: 10.1103/PhysRevLett.122.154501

[P169-2019] "High Performance of Carbon Nanotube Refrigerators"

Cantuario, T. E.*; Fonseca, A. F.*

Vapor-compression dominates the market for refrigeration devices due to low cost and relatively high efficiency. However, the most efficient vapor refrigerants are either ozone depleting or global warming substances. Solid-state cooling is a young field of research with promising results toward the development of new, efficient, and environment friendly technology for a new generation of refrigeration devices. One of these methods is based on the so-called elastocaloric effect (ECE), which consists of a temperature variation of a system in response to the application of adiabatic stresses. Although most of the literature describes the study of ECE solid-state cooling based on materials undergoing phase-transitions, a study recently predicted that carbon nanotubes (CNTs) present ECE as large as 30 K for 3% of strain. This motivates research toward the development of nanorefrigerators. As nobody knows the efficiency of such an ECE-based CNT nanorefrigerator, here, significantly high coefficient of performance values of 4.1 and 6.5, and extracted heat per weight as large as 40Jg(-1) are reported for a zigzag CNT nanorefrigerator operating in an Otto-like thermodynamic cycle. This efficiency is shown to overcome that of some other ECE materials.

ANNALEN DER PHYSIK [531], 4, 1800502, 2019. DOI: 10.1002/andp.201800502

[P170-2019] "Is every strong lens model unhappy in its own way? Uniform modelling of a sample of 13 quadruply+ imaged quasars"

Shajib, A. J.; Birrer, S.; Treu, T.; **Sobreira, F.***; et. al.

Strong-gravitational lens systems with quadruply imaged quasars (quads) are unique probes to address several fundamental problems in cosmology and astrophysics. Although they are intrinsically very rare, ongoing and planned wide-field deep-sky surveys are set to discover thousands of such systems in the next decade. It is thus paramount to devise a general framework to model strong-lens systems to cope with this large influx without being limited by expert investigator time. We propose such a general modelling framework (implemented with the publicly available software LENsTRoNotvrv) and apply it to uniformly model threeband Hubble Space Telescope Wide Field Camera 3 images of 13 quads. This is the largest uniformly modelled sample of quads to date and paves the way for a variety of studies. To illustrate the scientific content of the sample, we investigate the alignment between the mass and light distribution in the deflectors. The position angles of these distributions are wellaligned, except when there is strong external shear. However, we find no correlation between the ellipticity of the light and mass distributions. We also show that the observed flux-ratios between the images depart significantly from the predictions of simple smooth models. The departures are strongest in the bluest band, consistent with microlensing being the dominant cause in addition to millilensing. Future papers will exploit this rich data set in combination with ground-based spectroscopy and time delays to determine quantities such as the Ilubble constant, the free streaming length of dark matter, and the normalization of the initial stellar mass function.

MONTHLY NOTICES OF THE ROYAL ASTRONOMICAL SOCIETY [483], 4, 5649-5671, 2019. DOI: 10.1093/mnras/sty3397

[P171-2019] "Isospin-phonon coupling and Fano-interference in spin-orbit Mott insulator Sr2IrO4"

Samanta, K.*; Rigitano, D.*; Pagliuso, P. G.*; Granado, E.*

The "isospin-phonon" coupling in Sr2IrO4 is investigated by temperature dependent phonon Raman scattering. Anomalous behavior in the frequency of all studied optical phonons is observed below the magnetic transition temperature T-N similar to 240 K. The strongest effect is detected for the A(1g) mode at 272 cm(-1) associated with the modulation of the Ir-O-Ir bond angle. Additionally, the A(1g) mode at 560 cm(-1) shows a Fano asymmetric lineshape sensitive to T-N, supporting the existence of low energy (similar to 70 meV) electronic excitations that are renormalized by the magnetic order. These results reveal the characteristics of the interaction between the crystal lattice and electronic degrees of freedom in this "spin-orbit" entangled Mott insulator.

APPLIED PHYSICS LETTERS [114], 15, 152402, 2019. DOI: 10.1063/1.5094912

[P172-2019] "Jet fragmentation transverse momentum measurements from di-hadron correlations in root s7 TeV pp and root sNN=5.02 TeV p-Pb collisions"

Acharya, S.; Acosta, F. T.; Adamova, D.; **Albuquerque, D. S. D.*; Chinellato, D. D.*; De Souza, R. D.*; Takahashi, J.***; et. al.; ALICE Collaboration

The transverse structure of jets was studied via jet fragmentation transverse momentum (j(T)) distributions, obtained using two-particle correlations in proton-proton and proton--lead collisions, measured with the ALICE experiment at the LHC. The highest transverse momentum particle in each event is used as the trigger particle and the region 3 < p(Tt) < 15GeV/c is explored in this study. The measured distributions show a clear narrow Gaussian component and a wide non-Gaussian one. Based on Pythia simulations, the narrow component can be related to non-perturbative hadronization and the wide component to quantum chromodynamical splitting. The width of the narrow component shows a weak dependence on the transverse momentum of the trigger particle, in agreement with the expectation of universality of the hadronization process. On the other hand, the width of the wide component shows a rising trend suggesting increased branching for higher transverse momentum. The results obtained in pp collisions at root s TeV and in p-Pb collisions at root sNN=5.02 TeV are compatible within uncertainties and hence no significant cold nuclear matter effects are observed. The results are compared to previous measurements from CCOR and PHENIX as well as to Pythia 8 and Herwig 7 simulations.

JOURNAL OF HIGH ENERGY PHYSICS [3], 169, 2019. DOI: 10.1007/JHEP03(2019)169

[P173-2019] "Jet Shapes of Isolated Photon-Tagged Jets in Pb-Pb and pp Collisions at root S-NN=5.02 TeV"

Sirunyan, A. M.; Tumasyan, A.; Adam, W.; **Chinellato, J.*; Tonelli Manganote, E. J.***; et. al.; CMS Collaboration

The modification of jet shapes in Pb-Pb collisions, relative to those in pp collisions, is studied for jets associated with an isolated photon. The data were collected with the CMS detector at the LHC at a nucleon- nucleon center-of-mass energy of 5.02 TeV. Jet shapes are constructed from charged particles with track transverse momenta (p(T)) above 1 GeV/c in annuli around the axes of jets with p(T)(jet) > 30 GeV/c associated with an isolated photon with p(T)(gamma) > 60 GeV/c. The jet shape distributions are consistent between peripheral Pb-Pb and pp collisions, but are modified for more central Pb-Pb collisions.

In these central Pb-Pb events, a larger fraction of the jet momentum is observed at larger distances from the jet axis compared to pp, reflecting the interaction between the partonic medium created in heavy ion collisions and the traversing partons.

PHYSICAL REVIEW LETTERS [122], 15, 152001, 2019. DOI: 10.1103/PhysRevLett.122.152001

[P174-2019] "Magnetic structure and magnetoelastic coupling of GdNiSi3 and TbNiSi3"

Tartaglia, R.*; Arantes, F. R.; **Galdino, C. W.*; Rigitano, D.***; Kaneko, U. F.; Avila, M. A.; **Granado, E.***

The series of intermetallic compounds RNiSi3 (R = rare earth) shows interesting magnetic properties evolving with R and metamagnetic transitions under applied magnetic field for some of the compounds. The microscopic magnetic structures must be determined to rationalize such rich behavior. Here, resonant x-ray magnetic diffraction experiments are performed on single crystals of GdNiSi3 and TbNiSi3 at zero field. The primitive magnetic unit cell matches the chemical cell below the Neel temperatures T-N = 22.2 and 33.2 K, respectively. The magnetic structure is determined to be the same for both compounds (magnetic space group Cmmm'). It features ferromagnetic ac planes that are stacked in an antiferromagnetic + - + - pattern, with the rare-earth magnetic moments pointing along the (a) over arrow direction, which contrasts with the + - - + stacking and moment direction along the (b) over arrow axis previously reported for YbNiSi3. This indicates a sign reversal of the coupling constant between second-neighbor R planes as R is varied from Gd and Tb to Yb. The long b lattice parameter of GdNiSi3 and TbNiSi3 shows a magnetoelastic expansion upon cooling below T-N, pointing to the conclusion that the + - + - stacking is stabilized under lattice expansion. A competition between distinct magnetic stacking patterns with similar exchange energies tuned by the size of R sets the stage for the magnetic ground state instability observed along this series.

PHYSICAL REVIEW B [99], 9, 094428, 2019. DOI: 10.1103/PhysRevB.99.094428

[P175-2019] "Measurement and interpretation of differential cross sections for Higgs boson production at root s=13 TeV"

Sirunyan, A. M.; Tumasyan, A.; Adam, W.; **Chinellato, J. A*; Tonelli Manganote, E. J.***; et. al.; CMS Collaboration

Differential Higgs boson (H) production cross sections are sensitive probes for physics beyond the standard model. New physics may contribute in the gluon-gluon fusion loop, the dominant Higgs boson production mechanism at the LHC, and manifest itself through deviations from the distributions predicted by the standard model. Combined spectra for the H -> gamma gamma, H -> ZZ, and H -> b (b) over bar decay channels and the inclusive Higgs boson production cross section are presented, based on proton-proton collision data recorded with the CMS detector at root s = 13 TeV corresponding to an integrated luminosity of 35.9 fb(-1). The transverse momentum spectrum is used to place limits on the Higgs boson couplings to the top, bottom, and charm quarks, as well as its direct coupling to the gluon field. No significant deviations from the standard model are observed in any differential distribution. The measured total cross section is 61.1 +/- 6.0 (stat) +/- 3.7 (syst) pb, and the precision of the measurement of the differential cross section of the Higgs boson transverse momentum is improved by about 15% with respect to the H -> gamma gamma channel alone.

PHYSICS LETTERS B [792], 369-396, 2019. DOI: 10.1016/j.physletb.2019.03.059

[P176-2019] "Measurement compatibility in Bell nonlocality tests"

Temistocles, T.; **Rabelo, R.***; Cunha, M. T.

Incompatibility of observables, or measurements, is one of the key features of quantum mechanics, related, among other concepts, to Heisenberg's uncertainty relations and Bell nonlocality. In this manuscript we show, however, that even though incompatible measurements are necessary for the violation of any Bell inequality, some relevant Bell-like inequalities may be obtained if compatibility relations are assumed between the local measurements of one (or more) of the parties. Hence, compatibility of measurements is not necessarily a drawback and may, however, be useful for the detection of Bell nonlocality and device-independent certification of entanglement.

PHYSICAL REVIEW A [99], 4, 042120, 2019. DOI: 10.1103/PhysRevA.99.042120

[P177-2019] "Measurement of associated production of a W boson and a charm quark in proton-proton collisions at root s=13 Tev"

Sirunyan, A. M.; Tumasyan, A.; Adam, W.; **Chinellato, J. A.*; Tonelli Manganote, E. J.***; et. al.; CMS Collaboration

Measurements are presented of associated production of a W boson and a charm quark (W + c) in proton-proton collisions at a center-of-mass energy of 13 TeV. The data correspond to an integrated luminosity of 35.7 fb(-1) collected by the CMS experiment at the CERN LHC. The W bosons are identified by their decay into a muon and a neutrino. The charm quarks are tagged via the full reconstruction of D* (2010)(+/-) mesons that decay via D*(2010)(+/-) D-0 + pi(+/-) -> K--/+ + pi(+/-) + pi(+/-). A cross section is measured in the fiducial region defined by the muon transverse momentum p(T)(mu) > 26 GeV, muon pseudorapidity vertical bar eta(mu)vertical bar < 2.4, and charm quark transverse momentum p(T)(c) > 5 GeV. The inclusive cross section for this kinematic range is sigma(W + c) = 1026 +/- 31(stat)(-72)(+76) pb. The cross section is also measured differentially as a function of the pseudorapidity of the muon from the W boson decay. These measurements are compared with theoretical predictions and are used to probe the strange quark content of the proton.

EUROPEAN PHYSICAL JOURNAL C [79], 3, 269, 2019. DOI: 10.1140/epjc/s10052-019-6752-1

[P178-2019] "Measurement of D-0, D+, D+* and D-s(+) production in pp collisions at root s=5.02 TeV with ALICE"

Acharya, S.; Acosta, F. T.; Adamova, D.; **Albuquerque, D. S. D.*; Chinellato, D. D.*; De Souza, R. D.*; Takahashi, J.***; et. al.; ALICE Collaboration

The measurements of the production of prompt D0, D+, D+, and Ds+ mesons in proton-proton (pp) collisions at TeV with the ALICE detector at the Large Hadron Collider (LHC) are reported. D mesons were reconstructed at mid-rapidity (|y|<0.5) via their hadronic decay channels D0K-+, D+K-++, D+D0+K-++, Ds+phi+K+K-+, and their charge conjugates. The production cross sections were measured in the transverse momentum interval 0<pT<36 for D0, 1<pT<36 for D+ and D+, and in 2<pT<24 for Ds+ mesons. Thanks to the higher integrated luminosity, an analysis in finer pT bins with respect to the previous measurements at sTeV was performed, allowing for a more detailed description of the cross-section pT shape. The measured pT-differential production cross sections are compared to the results at s=7TeV and to four different perturbative QCD calculations. Its rapidity dependence is also tested combining the ALICE and LHCb measurements in pp collisions at s=5.02 TeV. This measurement will allow for a more accurate determination

of the nuclear modification factor in p-Pb and Pb-Pb collisions performed at the same nucleon-nucleon centre-of-mass energy.

EUROPEAN PHYSICAL JOURNAL C [79], 5, 388, 2019. DOI: 10.1140/epjc/s10052-019-6873-6

[P179-2019] "Measurement of exclusive Upsilon photoproduction from protons in pPb collisions at root sNN=5.02 Tev"

Sirunyan, A. M.; Tumasyan, A.; Adam, W.; **Chinellato, J.*; Tonelli Manganote, E. J.***; et. al.; CMS Collaboration

The exclusive photoproduction of (nS) meson states from protons, (nS) p (with n = 1, 2, 3), is studied in ultraperipheral pPb collisions at a centre-of-mass energy per nucleon pair of The measurement is performed using the decay mode, with data collected by the CMS experiment corresponding to an integrated luminosity of 32.6 nb(-1). Differential cross sections as functions of the nS) transverse momentum squared and rapidity y, are presented. The 1S) photoproduction cross section is extracted in the rapidity range < 2.2, which corresponds to photon-proton centre-of-mass energies in the range 91 W < 826 GeV. The data are compared to theoretical predictions based on perturbative quantum chromodynamics and to previous measurements.

EUROPEAN PHYSICAL JOURNAL C [79], 3, 277, 2019. DOI: 10.1140/epjc/s10052-019-6774-8

[P180-2019] "Measurement of inclusive very forward jet cross sections in proton-lead collisions at p sNN=5:02 TeV"

Sirunyan, A. M.; Tumasyan, A.; Adam, W.; **Chinellato, J. A.*; Tonelli Manganote, E. J.***; et. al.; CMS Collaboration

Measurements of di ff erential cross sections for inclusive very forward jet production in proton-lead collisions as a function of jet energy are presented. The data were collected with the CMS experiment at the LHC in the laboratory pseudorapidity range 6 : 6 < < 5 : 2. Asymmetric beam energies of 4TeV for protons and 1.58TeV per nucleon for Pb nuclei were used, corresponding to a center-of-mass energy per nucleon pair of p sNN = 5 : 02TeV. Collisions with either the proton (p+ Pb) or the ion (Pb+ p) traveling towards the negative hemisphere are studied. The jet cross sections are unfolded to stable-particle level cross sections with pT & 3 GeV, and compared to predictions from various Monte Carlo event generators. In addition, the cross section ratio of p+ Pb and Pb+ p data is presented. The results are discussed in terms of the saturation of gluon densities at low fractional parton momenta. None of the models under consideration describes all the data over the full jet--energy range and for all beam con fi gurations. Discrepancies between the di ff erential cross sections in data and model predictions of more than two orders of magnitude are observed.

JOURNAL OF HIGH ENERGY PHYSICS [5], 043, 2019. DOI: 10.1007/JHEP05(2019)043

[P181-2019] "Measurement of the energy density as a function of pseudorapidity in proton-proton collisions at root s=13 TeV"

Sirunyan, A. M.; Tumasyan, A.; Adam, W.; **Chinellato, J. A.*; Tonelli Manganote, E. J.***; et. al.; CMS Collaboration

A measurement of the energy density in proton-proton collisions at a centre-of-mass energy of sTeV is presented. The data have been recorded with the CMS experiment at the LHC during low luminosity operations in 2015. The energy density is studied as a function of pseudorapidity in the ranges -6.6<<-5.2 and 3.15<||<5.20. The results are compared with the predictions of several models. All the models considered suggest a different shape of the pseudorapidity dependence compared to that observed in the data. A comparison with LHC proton-proton collision data at s=0.9 and 7 TeV confirms the compatibility of the data with the hypothesis of limiting fragmentation.

EUROPEAN PHYSICAL JOURNAL C [79], 5, 391, 2019. DOI: 10.1140/epjc/s10052-019-6861-x

[P182-2019] "Measurement of the t(t)over-bar production cross section, the top quark mass, and the strong coupling constant using dilepton events in pp collisions at root s=13TeV"

Sirunyan, A. M.; Tumasyan, A.; Adam, W.; **Chinellato, J. A.*; Tonelli Manganote, E. J.***; et. al.; CMS Collaboration

A measurement of the top quark-antiquark pair production cross section sigma(t (t) over bar) in proton-proton collisions at a centre-of-mass energy of 13 TeV is presented. The data correspond to an integrated luminosity of 35.9 fb(-1), recorded by the CMS experiment at the CERN LHC in 2016. Dilepton events (e(+/-) mu(-/+), mu(+) mu(-), e(+) e(-)) are selected and the cross section is measured from a likelihood fit. For a top quark mass parameter in the simulation of m(t)(MC) = 172.5 GeV the fit yields a measured cross section sigma(t (t) over bar) = 803 +/- 2 (stat) +/- 25 (syst) +/- 20 (lumi) pb, in agreement with the expectation from the standard model calculation at next-to--next-to-leading order. A simultaneous fit of the cross section and the top quark mass parameter in the POWHEG simulation is performed. The measured value of m(t)(MC) = 172.33 +/- 0.14 (stat)(-0.72)(+0.66) (syst) GeV is in good agreement with previous measurements. The resulting cross section is used, together with the theoretical prediction, to determine the top quark mass and to extract a value of the strong coupling constant with different sets of parton distribution functions.

EUROPEAN PHYSICAL JOURNAL C [79], 5, 368, 2019. DOI: 10.1140/epjc/s10052-019-6863-8

[P183-2019] "Measurement of the top quark mass in the all-jets final state at root s=13 TeV and combination with the lepton plus jets channel"

Sirunyan, A. M.; Tumasyan, A.; Adam, W.; **Chinellato, J. A.*; Tonelli Manganote, E. J.***; et. al.; CMS Collaboration

A top quark mass measurement is performed using 35.9 fb - 1 of LHC proton- proton collision data collected with the CMS detector at v s = 13 TeV. The measurement uses the tt all-jets final state. A kinematic fit is performed to reconstruct the decay of the tt system and suppress themultijet background. Using the ideogram method, the top quark mass (mt) is determined, simultaneously constraining an additional jet energy scale factor (JSF). The resulting value of mt = 172.34 +/- 0.20 (stat+ JSF) +/- 0.70 (syst) GeV is in good agreement with previous measurements. In addition, a combined measurement that uses the tt lepton+ jets and all- jets final states is presented, using the same mass extraction method, and provides an mt measurement of 172.26 +/- 0.07 (stat+ JSF) +/- 0.61 (syst) GeV. This is the first combined mt extraction from the lepton+ jets and all- jets channels through a single likelihood function.

EUROPEAN PHYSICAL JOURNAL C [79], 4, 313, 2019. DOI: 10.1140/epjc/s10052-019-6788-2

[P184-2019] "Measurements of properties of the Higgs boson decaying to a Wboson pair in pp collisions at root s=13 TeV"

Sirunyan, A. M.; Tumasyan, A.; Adam, W.; **Chinellato, J. A.*; Tonelli Manganote, E. J.***; et. al.; CMS Collaboration

Measurements of the production of the standard model Higgs boson decaying to a W boson pair are reported. The W+ W- candidates are selected in events with an oppositely charged lepton pair, large missing transverse momentum, and various numbers of jets. To select Higgs bosons produced via vector boson fusion and associated production with a W or Z boson, events with two jets or three or four leptons are also selected. The event sample corresponds to an integrated luminosity of 35.9 fb(-1), collected in pp collisions at root s = 13 TeV by the CMS detector at the LHC during 2016. Combining all channels, the observed cross section times branching fraction is 1.28(-0.17)(+0.18) times the standard model prediction for the Higgs boson with a mass of 125.09 GeV. This is the first observation of the Higgs boson decay to W boson pairs by the CMS experiment.

PHYSICS LETTERS B [791], 96-129, 2019. DOI: 10.1016/j.physletb.2018.12.073

[P185-2019] "Measurements of the pp WZ inclusive and differential production cross sections and constraints on charged anomalous triple gauge couplings at s=13 TeV"

Sirunyan, A. M.; Tumasyan, A.; Adam, W.; **Chinellato, J. A.*; Tonelli Manganote, E. J.***; et. al.; CMS Collaboration

The WZ production cross section is measured in proton-proton collisions at a centre-of-mass energy = 13 TeV using data collected with the CMS detector, corresponding to an integrated luminosity of 35.9 fb(-1). The inclusive cross section is measured to be sigma(tot)(ppWZ)=48.0) pb, resulting in a total uncertainty of -2.78/+2.98 pb. Fiducial cross section and ratios of charge-dependent cross section measurements are provided. Differential cross section measurements are also presented with respect to three variables: the Z boson transverse momentum p(T), the leading jet p(T), and the M(WZ) variable, defined as the invariant mass of the system composed of the three leptons and the missing transverse momentum. Differential measurements with respect to the W boson p(T), separated by charge, are also shown. Results are consistent with standard model predictions, favouring next-to-next-to--leading-order predictions over those at next-to-leading order. Constraints on anomalous triple gauge couplings are derived via a binned maximum likelihood fit to the M(WZ) variable.

JOURNAL OF HIGH ENERGY PHYSICS [4], 122, 2019. DOI: 10.1007/JHEP04(2019)122

[P186-2019] "Mechanical Properties of Protomene: A Molecular Dynamics Investigation"

Oliveira, E. F.*; Autreto, P. A. S.; Woellner, C. F.; **Galvao, D. S.***

Recently, a new class of carbon allotrope called protomene was proposed. This new structure is composed of sp(2) and sp(3) carbon-bonds. Topologically, protomene can be considered as an sp(3) carbon structure (similar to 80% of this bond type) doped by sp(2) carbons. First-principles simulations have shown that protomene presents an electronic bandgap of similar to 3.4 eV. However, up to now, its mechanical properties have not been investigated. In this work, we have investigated protomene mechanical behavior under tensile strain through fully atomistic reactive molecular dynamics simulations using the ReaxFF force field, as available in the LAMMPS code. At room temperature, our results show that the protomene is very stable and the obtained ultimate strength and ultimate stress indicates an anisotropic behavior.The highest ultimate strength was obtained for the x-direction, with a value of similar to 110 GPa. As for the ultimate strain, the highest one was for the z-direction (similar to 25% of strain) before protomene mechanical fracture.

MRS ADVANCES [4], 3-4, 191-196, 2019. DOI: 10.1557/adv.2018.670

[P187-2019] "Mimicking the Hadamard discrete-time quantum walk with a time-independent Hamiltonian"

Moqadam, J. K.; **de Oliveira, M. C.***

The discrete-time quantum walk dynamics can be generated by a time-dependent Hamiltonian, repeatedly switching between the coin and the shift generators. We change the model and consider the case where the Hamiltonian is time-independent, including both the coin and the shift terms in all times. The eigenvalues and the related Bloch vectors for the time-independent Hamiltonian are then compared with the corresponding quantities for the effective Hamiltonian generating the quantum walk dynamics. Restricted to the non-localized initial quantum walk states, we optimize the parameters in the time--independent Hamiltonian such that it generates a dynamics similar to the Hadamard quantum walk. We find that the dynamics of the walker probability distribution and the corresponding standard deviation, the coin-walker entanglement, and the quantum-to-classical transition of the discrete-time quantum walk model can be approximately generated by the optimized time-independent Hamiltonian. We, further, show both dynamics are equivalent in the classical regime, as expected.

QUANTUM INFORMATION PROCESSING [18], 5, 141, 2019. DOI: 10.1007/s11128-019-2262-1

[P188-2019] "More out of less: an excess integrated Sachs--Wolfe signal from supervoids mapped out by the Dark Energy Survey"

Kovacs, A.; Sanchez, C.; Garcia-Bellido, J.; **Sobreira, F.***; et. al.; DES Collaboration

The largest structures in the cosmic web probe the dynamical nature of dark energy through their integrated Sachs-Wolfe imprints. In the strength of the signal, typical cosmic voids have shown good consistency with expectation A(ISW) = Delta T-data/Delta T-theory = 1, given the substantial cosmic variance. Discordantly, large-scale hills in the gravitational potential, or supervoids, have shown excess signals. In this study, we mapped out 87 new supervoids in the total 5000 deg(2) footprint of the Dark Energy Survey at $0.2 < z < 0.9$ to probe these anomalous claims. We found an excess imprinted profile with A(ISW) approximate to 4.1 +/- 2.0 amplitude. The combination with independent BOSS data reveals an ISW imprint of supervoids at the 3.3 sigma significance level with an enhanced A(ISW) approximate to 5.2 +/- 1.6 amplitude. The tension with Lambda CDM predictions is equivalent to 2.6 sigma and remains unexplained.

MONTHLY NOTICES OF THE ROYAL ASTRONOMICAL SOCIETY [484], 4, 5267-5277, 2019. DOI: 10.1093/mnras/stz341

[P189-2019] "Multi-Messenger Physics With the Pierre Auger Observatory"

Kampert, K. H.; Mostafa, M. A.; Zas, E.; **Chinellato, J. A.*; Daniel, B.*; Castro, M. L. Diaz*; Dobrigkeit, C.*; Fauth, A. C.*; Muller, M. A.*; Pereira, L. A. S.***; et. al.; Pierre Auger Collaboration

An overview of the multi-messenger capabilities of the Pierre Auger Observatory is presented. The techniques and performance of searching for Ultra-High Energy neutrinos, photons and neutrons are described. Some of the most relevant results are reviewed, such as stringent upper bounds that were placed to a flux of diffuse cosmogenic neutrinos and photons, bounds placed on neutrinos emitted from compact binary mergers that were detected by LIGO and Virgo during their first and second observing runs, as well as searches for high energy photons and neutrons from the Galactic center that constrain the properties of the putative Galactic PeVatron, observed by the H.E.S.S. collaboration.

The observation of directional correlations between ultra--high energy cosmic rays and either high energy astrophysical neutrinos or specific source populations, weighted by their electromagnetic radiation, are also discussed. They constitute additional multi-messenger approaches aimed at identifying the sources of high energy cosmic rays.

FRONTIERS IN ASTRONOMY AND SPACE SCIENCES [6], 24, 2019. DOI: 10.3389/fspas.2019.00024

[P190-2019] "Nonperturbative Ball-Chiu construction of the three-gluon vertex"

Aguilar, A. C.*; Ferreira, M. N.*; Figueiredo, C. T.*; Papavassiliou, J.

We present the detailed derivation of the longitudinal part of the three-gluon vertex from the Slavnov-Taylor identities that it satisfies, by means of a nonperturbative implementation of the Ball-Chiu construction; the latter, in its original form, involves the inverse gluon propagator, the ghost dressing function, and certain form factors of the ghost-gluon kernel. The main conceptual subtlety that renders this endeavor nontrivial is the infrared finiteness of the gluon propagator, and the resulting need to separate the vertex into two pieces, one that is intimately connected with the emergence of a gluonic mass scale, and one that satisfies the original set of Slavnov-Taylor identities, but with the inverse gluon propagator replaced by its "kinetic" term. The longitudinal form factors obtained by this construction are presented for arbitrary Euclidean momenta, as well as special kinematic configurations, parametrized by a single momentum. A particularly preeminent feature of the components comprising the tree-level vertex is their considerable suppression for momenta below 1 GeV, and the appearance of the characteristic "zero-crossing" in the vicinity of 100-200 MeV. Special combinations of the form factors derived with this method are compared with the results of recent large-volume lattice simulations, and are found to capture faithfully the rather complicated curves formed by the data. A similar comparison with results obtained from Schwinger-Dyson equations reveals a fair overall agreement, but with appreciable differences at intermediate energies. A variety of issues related to the distribution of the pole terms responsible for the gluon mass generation are discussed in detail, and their impact on the structure of the transverse parts is elucidated. In addition, a brief account of several theoretical and phenomenological possibilities involving these newly acquired results is presented.

PHYSICAL REVIEW D [99], 9, 094010, 2019. DOI: 10.1103/PhysRevD.99.094010

[P191-2019] "Normalized glandular dose (DgN) coefficients from experimental mammographic x-ray spectra"

Santos, J. C.; **Tomal, A.*;** de Barros, N.; Costa, P. R.

Mean glandular dose is the quantity used for dosimetry in mammography and depends on breast-related characteristics, such as thickness and density, and on the x-ray spectrum used for breast imaging. This work aims to present an experimentally--based method to derive polyenergetic normalized glandular dose coefficients (DgN(p)) from the spectral difference between x-ray spectra incident and transmitted through breast phantoms with glandular/adipose proportions of 30/70 and 50/50 and thicknesses up to 4.5 cm. The spectra were produced by a Mammomat 3000 Nova system using radiographic techniques commonly applied for imaging compressed breast thickness lower than 6 cm (Mo/Mo, Mo/Rh and W/Rh spectra at 26 and 28 kVp). DgN(p) coefficients were compared with values estimated using Boones' method and data from breast images (DICOM Organ Dose and VolparaDose calculations). The DgN(p) were also evaluated in layers into the phantoms (depth-DgN(p)) using both x-ray spectra and thermoluminescent dosimeters (TLD-100). Maximum differences between DgN(p) from the method presented in this study and results using Boone's method was 11%, with larger differences for Mo/Rh spectra in relation to the Mo/Mo. The DgN(p) maximum differences to the coefficients obtained using patient images were 8.0%, for the DgN calculated using Volpara and 6.4% for the DgN from DICOM Organ Dose, for a 4.5 cm breast phantom with 30% glandularity. The DgN(p) estimated from the depth-DgN(p) distributions differ up to 5.2% to the coefficients obtained using the pair incident-transmitted spectra to calculate the DgN(p) directly in the whole phantom. The depth-DgN(p) distributions estimated with TLDs were consistent with the results observed using the experimental spectra, with maximum difference of 3.9%. In conclusion, polyenergetic x-ray spectrometry proved to be an applicable tool for research in dosimetry in mammography allowing spectral characterization. This approach can also be useful for investigation of the influence of x-ray spectra on glandular dose.

PHYSICS IN MEDICINE AND BIOLOGY [64], 10, 105010, 2019. DOI: 10.1088/1361-6560/ab171a

[P192-2019] "Observation of prompt J/psi meson elliptic flow in high-multiplicity pPb collisions at root s(NN)=8.16 TeV"

Sirunyan, A. M.; Tumasyan, A.; Adam, W.; **Chinellato, J. A.*; Tonelli Manganote, E. J.***; et. al.; CMS Collaboration

A measurement of the elliptic flow (v(2)) of prompt J/psi mesons in high-multiplicity pPbcollisions is reported using data collected by the CMS experiment at a nucleon-nucleon center--of-mass energy root s(NN)= 8.16 TeV. Prompt J/psi mesons decaying into two muons are reconstructed in the rapidity region in the nucleon-nucleon center-of-mass frame (y(cm)), corresponding to either -2.86 < y(cm) < -1.86 or 0.94 < y(cm)< 1.94. The average v(2) result from the two rapidity ranges is reported over the transverse momentum (p(T)) range from 0.2 to 10 GeV. Positive v(2) values are observed for the prompt J/psi meson, as extracted from long-range two-particle correlations with charged hadrons, for 2 < p(T) < 8 GeV. The prompt J/psi results are compared with previous CMS measurements of elliptic flow for open charm mesons (D-0) and strange hadrons. From these measurements, constraints can be obtained on the collective dynamics of charm quarks produced in high-multiplicity events arising from small systems.

PHYSICS LETTERS B [791], 172-194, 2019. DOI: 10.1016/j.physletb.2019.02.018

[P193-2019] "Observation of Single Top Quark Production in Association with a Z Boson in Proton-Proton Collisions at root s=13 TeV"

Sirunyan, A. M.; Tumasyan, A.; Adam, W.; **Chinellato, J. A.*; Tonelli Manganote, E. J.***; et. al.; CMS Collaboration

The observation of single top quark production in association with a Z boson and a quark (tZq) is reported. Events from proton-proton collisions at a center-of-mass energy of 13 TeV containing three charged leptons (either electrons or muons) and at least two jets are analyzed. The data were collected with the CMS detector in 2016 and 2017 and correspond to an integrated luminosity of 77.4fb(-1). The increased integrated luminosity, a multivariate lepton identification, and a redesigned analysis strategy improve significantly the sensitivity of the analysis compared to previous searches for tZq production. The tZq signal is observed with a significance well over 5 standard deviations. The measured tZq production cross section is sigma(pp -> tZq -> tl(+) l(-) q) = 111 +/- 13 (stat)(-9) (+11) (syst) fb, for dilepton invariant masses above 30 GeV,

in agreement with the standard model expectation.

PHYSICAL REVIEW LETTERS [122], 13, 132003, 2019. DOI: 10.1103/PhysRevLett.122.132003

[P194-2019] "Observation of Two Excited B-c(+) States and Measurement of the B-c(+) (2S) Mass in pp Collisions at root s=13 TeV"

Sirunyan, A. M.; Tumasyan, A.; Adam, W.; **Chinellato, J. A.*; Tonelli Manganote, E. J.***; et. al.; CMS Collaboration

Signals consistent with the B-c(+)(2S) and B-c*(+)(2S) states are observed in proton-proton collisions at root s = 13 TeV, in an event sample corresponding to an integrated luminosity of 143 fb(-1), collected by the CMS experiment during the 2015-2018 LHC running periods. These excited (b) over barc states are observed in the B-c(+)pi(+)pi(-) invariant mass spectrum, with the ground state B-c(+) reconstructed through its decay to J/psi pi(+). The two states are reconstructed as two well-resolved peaks, separated in mass by 29.1 +/- 1.5(stat) +/- 0.7(syst) MeV. The observation of two peaks, rather than one, is established with a significance exceeding five standard deviations. The mass of the B-c(+)(2S) meson is measured to be 6871.0 +/- 1.2(stat) +/- 0.8(syst) +/- 0.8(B-c(+)) MeV, where the last term corresponds to the uncertainty in the world-average B-c(+) mass.

PHYSICAL REVIEW LETTERS [122], 13, 132001, 2019. DOI: 10.1103/PhysRevLett.122.132001

[P195-2019] "On the mechanical properties of protomene: A theoretical investigation"

Oliveira, E. F.*; Autreto, P. A. S.*; Woellner, C. F.*; Galvao, D. S.*

We report a detailed study through fully atomistic molecular dynamics simulations and DFT calculations on the mechanical properties of protomene. Protomene is a new carbon allotrope composed of a mixture of sp(2) and sp(3) hybridized states. Our results indicate that protomene presents an anisotropic behavior about tensile deformations. At room temperature, protomene presents an ultimate strength of similar to 100 GPa and Young's modulus of similar to 600 GPa, lower than the same for other carbon allotropes. Despite that, protomente presents the highest ultimate strain along the z--direction (similar to 24.7%). Our results also show that stretching the protomene along the z-direction or heating it can induce a semiconductor-metallic phase transition, due to a high amount of sp(3) bonds that are converted to sp(2) ones.

COMPUTATIONAL MATERIALS SCIENCE [161], 190-198, 2019. DOI: 10.1016/j.commatsci.2019.01.050

[P196-2019] "pH-dependent X-ray Photoelectron Chemical Shifts and Surface Distribution of Cysteine in Aqueous Solution"

Carravetta, V.; **Gomes, A. H. D.***; Monti, S.; Mocellin, A.; Marinho, R. R. T.; Bjorneholm, O.; Agren, H.; **de Brito, A. N.***

The distribution and protonation states of amino acids in water droplets are of considerable concern in studies on the formation of clouds in the atmosphere as well as in many biological contexts. In the present work we use the amino acid cysteine as a prototypical example and explore the protonation states of this molecule in aqueous solution, which are strongly affected by the acidity of the environment and also can show different distributions between surface and bulk. We use a combination of X-ray photoelectron chemical shift measurements, density functional theory calculations of the shifts, and reactive force field molecular dynamics simulations of the underlying structural dynamics. We explore how the photoelectron spectra distinctly reflect the different protonation states that are generated by variation of the solution acidity and how the distribution of these protonation states can differ between bulk and surface regions. At specific pH values, we find that the distribution of the cysteine species at the surface is quite different from that in bulk, in particular, for the appearance in the surface region of species which do not exist in bulk. Some ramifications of this finding are discussed.

JOURNAL OF PHYSICAL CHEMISTRY B [123], 17, 3776-3785, 2019. DOI: 10.1021/acs.jpcb.9b00866

[P197-2019] "Phase resolved method using the Hill-Climbing Metaheuristic Algorithm applied for the spectral separation from photoacoustic spectra of chilli pepper skin and yellow corn pericarp"

Jaime, J.; Hernandez-Wong, J.; Nogal, U.; Rojas, A.; Calderon, A.; Rojas-Trigos, J. B.; Munoz, R.; Juarez-Gracia, G.; **Mansanares, A. M.***; Marin, E.

The phase-resolved method has been widely used in photoacoustic spectroscopy for separating the contribution of different optical absorption centers to a spectrum. However, the procedure is lengthy, tedious and without precision control, because one has to calculate several spectra to search for the phase angle at which only one contribution is present every time. In this work, this limitation is avoided by the implementation of a method as a search and optimization problem using the Hill Climbing Metaheuristic Algorithm. As test examples, the photoacoustic spectra of chilli fruit skin of Anaheim type (Capsicum Annuum L.) and yellow corn grain pericarp of dent type (Zea Mays L.) were analyzed in the wavelength ranges where there is optical absorption of the photoprotective pigments of these samples.

MEASUREMENT [138], 143-148, 2019. DOI: 10.1016/j.measurement.2019.02.012

[P198-2019] "Phase Transitions in Phospholipid Monolayers: Theory Versus Experiments"

de Oliveira, F. O.*; Tamashiro, M. N.*

The Doniach lattice gas (DLG) represents a ternary-mixture statistical model, whose components, water molecules (w), ordered-chain lipids (o), and disordered-chain lipids (d)-the latter carrying a high degenerescence omega >> 1-are located at each site of a two-dimensional lattice. The DLG model was introduced to describe phospholipid Langmuir films at the air--water interface and can be mapped into a spin-1 model, with the single-site states s(i) = 0, +1, and -1 representing the three types of molecules in the system (w, o, and d), respectively. The model allows lipid-density fluctuations and has been analyzed at the mean-field approximation (Guidi, H. S.; Henriques, V. B. Phys. Rev. E 2014, 90, 052705) as well as at the pair approximation (de Oliveira, F. O.; Tamashiro, M. N. Phys. Rev. E 2019, 99, 012147). In this work, we focus on performing an explicit comparison of the theoretical predictions obtained for the DLG model at the pair approximation with isothermal monolayer compression experiments (Nielsen, L. K.; Bjernholm, T.; Mouritsen, 0. G. Langmuir 2007, 23, 11684) for the two most commonly studied saturated zwitterionic phospholipids, DMPC (1,2-dimyristoyl-sn-glycero-3-phosphocholine) and DPPC (1,2-dipalmitoyl-sn-glycero-3-phosphocholine). The model parameters obtained by fitting to the experimental data yield phase diagrams that are qualitatively consistent with the observed phase transitions on DMPC and DPPC monolayers, with the absence of a low-density gas phase. Quantitative agreement, however, was less significant partially because of the challenging reproducibility of Langmuir monolayer compression experiments, claimed in the literature to be influenced by kinetic effects.

LANGMUIR [35], 10, 3848-3858, 2019. DOI: 10.1021/acs.langmuir.8b03244

[P199-2019] "Rediscovery of the Sixth Star Cluster in the Fornax Dwarf Spheroidal Galaxy"

Wang, M. Y.; Koposov, S.; Drlica-Wagner, A.; **Sobreira, F.***; et. al.; DES Collaboration

Since first noticed by Shapley in 1939, a faint object coincident with the Fornax dwarf spheroidal has long been discussed as a possible sixth globular cluster (GC) system. However, debate has continued over whether this overdensity is a statistical artifact or a blended galaxy group. In this Letter we demonstrate, using deep DECam imaging data, that this object is well resolved into stars and is a bona fide star cluster. The stellar overdensity of this cluster is statistically significant at the level of similar to 6-6.7 sigma in several different photometric catalogs including Gaia. Therefore, it is highly unlikely to be caused by random fluctuation. We show that Fornax 6 is a star cluster with a peculiarly low surface brightness and irregular shape, which may indicate a strong tidal influence from its host galaxy. The Hess diagram of Fornax 6 is largely consistent with that of Fornax field stars, but it appears to be slightly bluer. However, it is still likely more metal-rich than most of the GCs in the system. Faint clusters like Fornax 6 that orbit and potentially get disrupted in the centers of dwarf galaxies can prove crucial for constraining the dark matter distribution in Milky Way satellites.

ASTROPHYSICAL JOURNAL LETTERS [875], 2, L13, 2019. DOI: 10.3847/2041-8213/ab14f5

[P200-2019] "Regioregularity and deposition effect on the physical/chemical properties of polythiophene derivatives films"

Roncaselli, L. K. M.; Silva, E. A.; **Braunger, M. L.***; Souza, N. C.; Ferreira, M.; De Santana, H.; Olivati, C. A.

Polythiophene thin films are widely studied for applications in organic electronics. However, some comparisons are still missing, regarding distinct deposition techniques and regioregularity. Here regioregular and regiorandom alkyl-substituted polythiophene derivatives (P3ATs) were deposited on solid substrates using both Langmuir-Blodgett (LB) and Langmuir--Schaefer (LS) techniques. The main goal was to verify the possible influence of the regioregularity as well the deposition technique on their optical, electrical and electrochemical properties. LB and LS films of regioregular and regiorandom poly(3-butylthiophene) (P3BT) and poly(3-octylthiophene) (P3OT) were deposited onto glass/Indium-Tin-Oxide) substrates and characterized by UV-visible optical spectroscopy, atomic force microscopy, cyclic voltammetry, and conductivity measurements. The results demonstrated the influence of the deposition technique on the electrical outcome, moreover, the regioregularity affected all the performed characterizations. In addition, this paper may be useful to understand how the amphiphilic molecule addition affected the film properties of regioregular and regiorandom P3ATs, particularly the energy diagram provided by the electrochemical and absorption features.

NANOTECHNOLOGY [30], 32, 325703, 2019. DOI: 10.1088/1361-6528/ab19f0

[P201-2019] "Resonant amplification via Er-doped clad Si photonic molecules: Towards compact low-loss/high-Q Si photonic devices"

Jarschel, P. F.*; Frateschi, N. C.*

Silicon photonics routers and band-pass filters employing ring resonators are usually constrained by a trade-off between quality factors and insertion loss, which is even more pronounced in compact designs. Device real estate is another factor to be considered for compactness and cost reduction. We propose an approach to simultaneously reduce insertion losses and increase the quality factor in such devices, while minimizing footprint. This approach consists in replacing the standard SiO2 top cladding of Si devices by erbium-doped Al2O3 films with a single post-processing step. Experimental results confirm the effectiveness of the method, where 1 dB output power increase is observed for a single ring device, in addition to an increase of 5% in the Q factor. In some cases of structures comprised of multiple coupled resonators, i.e., photonic molecules, the observed value of power increase is as high as 2.6 dB, with a Q factor increase of 25% and loss reduction of 3 dB.

SOLID-STATE ELECTRONICS [155], 144-149, 2019. DOI: 10.1016/j.sse.2019.03.016

[P202-2019] "Roles of Precursor Conformation and Adatoms in Ullmann Coupling: An Inverted Porphyrin on Cu(111)"

Moreno-Lopez, J. C.; Mowbray, D. J.; Paz, A. P.; **de Ferreira, R. C. D.*; dos Santos, A. C.*;** Ayala, P.; **de Siervo, A.***

Surface diffusion, molecular conformation, and on-surface coupling reactions are key processes for building tailored molecular nanostructures such as graphene nanoribbons, polycyclic aromatic hydrocarbons, and one-dimensional/two--dimensional (2D) polymers. Here, we study the surface diffusion and coupling in situ of a chlorinated porphyrin, namely 5,10,15,20-tetrakis(4-chlorophenyl)porphyrin (Cl4TPP), using a combined scanning tunneling microscopy (STM), density functional theory (DFT), and X-ray photoelectron spectroscopy approach. Using STM, we obtain surface migration and rotation barriers Delta E of 0.77 +/- 0.09 and 0.93 +/- 0.28 eV, respectively, indicative of covalent binding to the surface. In fact, we find that the precursors as well as all the reaction species exclusively (approximate to 100%) adopt a peculiar "inverted" conformation covalently bonded to Cu(111). Using DFT, we have mapped two coupling reaction pathways: direct dechlorination and Cu adatom-mediated Ullmann coupling. We find that the latter is essentially barrierless, whereas the former faces a barrier of about 0.9 eV for inverted Cl4TPP on Cu(111). Our STM measurements show that C-Cu-C organometallic species are the main final products in the presence of Cu adatoms, which is explained by our DFT reaction profile when heat dissipation to the substrate is taken into account. This work not only highlights the relevance of surface adatoms in selecting the reaction pathway but also opens the possibility of precisely tailoring 2D molecular assemblies by controlling the supply of Cu adatoms.

CHEMISTRY OF MATERIALS [31], 8, 3009-3017, 2019. DOI: 10.1021/acs.chemmater.9b00668

[P203-2019] "Search for a W ' boson decaying to a tau lepton and a neutrino in proton-proton collisions at root s=13 TeV"

Sirunyan, A. M.; Tumasyan, A.; Adam, W.; **Chinellato, J. A.*; Tonelli Manganote, E. J.*;** et. al.; CMS Collaboration

A search for a new high-mass resonance decaying to a tau lepton and a neutrino is reported. The analysis uses proton-proton collision data collected by the CMS experiment at the LHC at root s= 13 TeV, corresponding to an integrated luminosity of 35.9 fb(-1). The search utilizes hadronically decaying tau leptons. No excess in the event yield is observed at high transverse masses of the tau and missing transverse momentum. An interpretation of results within the sequential standard model excludes W' boson masses below 4.0 TeV at 95% confidence level.

Existing limits are also improved on models in which the W' boson decays preferentially to fermions of the third generation. Heavy W' bosons with masses less than 1.7-3.9 TeV, depending on the coupling in the non-universal G(221) model, are excluded at 95% confidence level. These are the most stringent limits on this model to date.

PHYSICS LETTERS B [792], 107-131, 2019. DOI: 10.1016/j.physletb.2019.01.069

[P204-2019] "Search for a W boson decaying to a vector-like quark and a top or bottom quark in the all-jets final state"

Sirunyan, A. M.; Tumasyan, A.; Adam, W.; **Chinellato, J. A.*; Tonelli Manganote, E. J.***; et. al.; CMS Collaboration

A search for a heavy W resonance decaying to one B or T vector-like quark and a top or bottom quark, respectively, is presented. The search uses proton-proton collision data collected in 2016 with the CMS detector at the LHC, corresponding to an integrated luminosity of 35.9 fb(-1) at 13 TeV. Both decay channels result in a final state with a top quark, a Higgs boson, and a b quark, each produced with significant energy. The all-hadronic decays of both the Higgs boson and the top quark are considered. The final-state jets, some of which correspond to merged decay products of a boosted top quark and a Higgs boson, are selected using jet substructure techniques, which help to suppress standard model backgrounds. A W boson signal would appear as a narrow peak in the invariant mass distribution of these jets. No significant deviation in data with respect to the standard model background predictions is observed. Cross section upper limits on W boson production in the top quark, Higgs boson, and b quark decay mode are set as a function of the W mass, for several vector-like quark mass hypotheses. These are the first limits for W boson production in this decay channel, and cover a range of 0.01 to 0.43 pb in the W mass range between 1.5 and 4.0 TeV.

JOURNAL OF HIGH ENERGY PHYSICS [3], 127, 2019. DOI: 10.1007/JHEP03(2019)127

[P205-2019] "Search for an L-mu - L-tau gauge boson using Z -> 4 mu events in proton-proton collisions at root s=13 TeV"

Sirunyan, A. M.; Tumasyan, A.; Adam, W.; **Chinellato, J. A.*; Tonelli Manganote, E. J.***; et. al.; CMS Collaboration

A search for a narrow Z' gauge boson with a mass between 5 and 70 GeV resulting from an L-mu - L-tau U (1) local gauge symmetry is reported. Theories that predict such a particle have been proposed as an explanation of various experimental discrepancies, including the lack of a dark matter signal in direct-detection experiments, tension in the measurement of the anomalous magnetic moment of the muon, and reports of possible lepton flavor universality violation in B meson decays. A data sample of proton-proton collisions at a center-of-mass energy of 13 TeV is used, corresponding to an integrated luminosity of 77.3 fb(-1) recorded in 2016 and 2017 by the CMS detector at the LHC. Events containing four muons with an invariant mass near the standard model Z boson mass are analyzed, and the selection is further optimized to be sensitive to the events that may contain Z -> Z'mu mu -> 4 mu decays. The event yields are consistent with the standard model predictions. Upper limits of 10(-8)-10(-7) at 95% confidence level are set on the product of branching fractions B(Z -> Z'mu mu)B(Z' -> mu mu), depending on the Z' mass, which excludes a Z' boson coupling strength to muons above 0.004-0.3. These are the first dedicated limits on L-mu - L-tau models at the LHC and result in a significant increase in the excluded model parameter space. The results of this search may also be used to constrain the coupling strength of any light Z' gauge boson to muons.

PHYSICS LETTERS B [792], 345-368, 2019. DOI: 10.1016/j.physletb.2019.01.072

[P206-2019] "Search for contact interactions and large extra dimensions in the dilepton mass spectra from proton--proton collisions at root s=13 TeV"

Sirunyan, A. M.; Tumasyan, A.; Adam, W.; **Chinellato, J. A.*; Tonelli Manganote, E. J.***; et. al.; CMS Collaboration

A search for nonresonant excesses in the invariant mass spectra of electron and muon pairs is presented. The analysis is based on data from proton-proton collisions at a center-of-mass energy of 13 TeV recorded by the CMS experiment in 2016, corresponding to a total integrated luminosity of 36 fb(-1). No significant deviation from the standard model is observed. Limits are set at 95% confidence level on energy scales for two general classes of nonresonant models. For a class of fermion contact interaction models, lower limits ranging from 20 to 32 TeV are set on the characteristic compositeness scale . For the Arkani-Hamed, Dimopoulos, and Dvali model of large extra dimensions, the first results in the dilepton final state at 13 TeV are reported, and values of the ultraviolet cutoff parameter (T) below 6.9 TeV are excluded. A combination with recent CMS diphoton results improves this exclusion to (T) below 7.7 TeV, providing the most sensitive limits to date in nonhadronic final states.

JOURNAL OF HIGH ENERGY PHYSICS [4], 114, 2019. DOI: 10.1007/JHEP04(2019)114

[P207-2019] "Search for dark matter produced in association with a Higgs boson decaying to a pair of bottom quarks in proton-proton collisions at root s=13TeV"

Sirunyan, A. M.; Tumasyan, A.; Adam, W.; **Chinellato, J. A.*; Tonelli Manganote, E. J.***; et. al.; CMS Collaboration

A search for dark matter produced in association with a Higgs boson decaying to a pair of bottom quarks is performed in proton-proton collisions at a center-of-mass energy of 13 TeV collected with the CMS detector at the LHC. The analyzed data sample corresponds to an integrated luminosity of 35.9 fb(-1). The signal is characterized by a large missing transverse momentum recoiling against a bottom quark-antiquark system that has a large Lorentz boost. The number of events observed in the data is consistent with the standard model background prediction. Results are interpreted in terms of limits both on parameters of the type-2 two-Higgs doublet model extended by an additional light pseudoscalar boson a (2HDM+a) and on parameters of a baryonic Z simplified model. The 2HDM+a model is tested experimentally for the first time. For the baryonic Z model, the presented results constitute the most stringent constraints to date.

EUROPEAN PHYSICAL JOURNAL C [79], 3, 280, 2019. DOI: 10.1140/epjc/s10052-019-6730-7

[P208-2019] "Search for dark matter produced in association with a single top quark or a top quark pair in proton--proton collisions at s=13 TeV"

Sirunyan, A. M.; Tumasyan, A.; Adam, W.; **Chinellato, J. A.*; Tonelli Manganote, E. J.***; et. al.; CMS Collaboration

A search for dark matter produced in association with top quarks in proton-proton collisions at a center-of-mass energy of 13 TeV is presented. The data set used corresponds to an integrated luminosity of 35.9 fb(-1) recorded with the CMS detector at the LHC. Whereas previous searches for neutral scalar or pseudoscalar mediators considered dark matter production in association with a top quark pair only,

this analysis also includes production modes with a single top quark. The results are derived from the combination of multiple selection categories that are defined to target either the single top quark or the top quark pair signature. No significant deviations with respect to the standard model predictions are observed. The results are interpreted in the context of a simplified model in which a scalar or pseudoscalar mediator particle couples to a top quark and subsequently decays into dark matter particles. Scalar and pseudoscalar mediator particles with masses below 290 and 300 GeV, respectively, are excluded at 95% confidence level, assuming a dark matter particle mass of 1 GeV and mediator couplings to fermions and dark matter particles equal to unity.

JOURNAL OF HIGH ENERGY PHYSICS [3], 141, 2019. DOI: 10.1007/JHEP03(2019)141

[P209-2019] "Search for excited leptons in final states in proton-proton collisions at root s=13 TeV"

Sirunyan, A. M.; Tumasyan, A.; Adam, W.; **Chinellato, J. A.*; Tonelli Manganote, E. J.***; et. al.; CMS Collaboration

A search is presented for excited electrons and muons in final states at the LHC. The search is based on a data sample corresponding to an integrated luminosity of 35.9 fb(-1) of proton-proton collisions at a center-of-mass energy of 13 TeV, collected with the CMS detector in 2016. This is the first search for excited leptons at = 13 TeV. The observation is consistent with the standard model background prediction, and the most stringent exclusion limits to date are set on the excited lepton mass and the compositeness scale, at 95% confidence level. Excited electrons and muons are excluded for masses below 3.9 and 3.8 TeV, respectively, under the assumption that the excited lepton mass equals the compositeness scale. The best observed limit on the compositeness scale is obtained with an excited lepton mass of around 1.0 TeV, excluding values below 25 TeV for both excited electrons and muons.

JOURNAL OF HIGH ENERGY PHYSICS [4], 015, 2019. DOI: 10.1007/JHEP04(2019)015

[P210-2019] "Search for heavy neutrinos and third-generation leptoquarks in hadronic states of two leptons and two jets in proton-proton collisions at root s=13 TeV"

Sirunyan, A. M.; Tumasyan, A.; Adam, W.; **Chinellato, J. A.*; Tonelli Manganote, E. J.***; et. al.; CMS Collaboration

A search for new particles has been conducted using events with two high transverse momentum leptons that decay hadronically and at least two energetic jets. The analysis is performed using data from proton-proton collisions at 13 TeV, collected by the CMS experiment at the LHC in 2016 and corresponding to an integrated luminosity of 35.9 fb(-1). The observed data are consistent with standard model expectations. The results are interpreted in the context of two physics models. The first model involves right-handed charged bosons, W-R, that decay to heavy right-handed Majorana neutrinos, N (= e, ,), arising in a left-right symmetric extension of the standard model. The model considers that N-e and N are too heavy to be detected at the LHC. Assuming that the N mass is half of the W-R mass, masses of the W-R boson below 3.50 TeV are excluded at 95% confidence level. Exclusion limits are also presented considering different scenarios for the mass ratio between N and W-R, as a function of W-R mass. In the second model, pair production of third-generation scalar leptoquarks that decay into bb is considered, resulting in an observed exclusion region with leptoquark masses below 1.02 TeV, assuming a 100% branching fraction for the leptoquark decay to a lepton and a bottom quark. These results represent the most stringent limits to date on these models.

JOURNAL OF HIGH ENERGY PHYSICS [3], 170, 2019. DOI: 10.1007/JHEP03(2019)170

[P211-2019] "Search for nonresonant Higgs boson pair production in the b(b)over-barb(b)over-bar final state at root s=13 TeV"

Sirunyan, A. M.; Tumasyan, A.; Adam, W.; **Chinellato, J. A.*; Tonelli Manganote, E. J.***; et. al.; CMS Collaboration

Results of a search for nonresonant production of Higgs boson pairs, with each Higgs boson decaying to a b (b) over bar pair, are presented. This search uses data from proton-proton collisions at a centre-of-mass energy of 13 TeV, corresponding to an integrated luminosity of 35.9 fb(-1), collected by the CMS detector at the LHC. No signal is observed, and a 95% confidence level upper limit of 847 fb is set on the cross section for standard model nonresonant Higgs boson pair production times the squared branching fraction of the Higgs boson decay to a b (b) over bar pair. The same signature is studied, and upper limits are set, in the context of models of physics beyond the standard model that predict modified couplings of the Higgs boson.

JOURNAL OF HIGH ENERGY PHYSICS [4], 112, 2019. DOI: 10.1007/JHEP04(2019)112

[P212-2019] "Search for pair production of first-generation scalar leptoquarks at root s=13 TeV"

Sirunyan, A. M.; Tumasyan, A.; Adam, W.; **Chinellato, J. A.*; Tonelli Manganote, E. J.***; et. al.; CMS Collaboration

A search for the pair production of first-generation scalar leptoquarks is performed using proton-proton collision data recorded at 13 TeV center-of-mass energy with the CMS detector at the LHC. The data correspond to an integrated luminosity of 35.9 fb(-1). The leptoquarks are assumed to decay promptly to a quark and either an electron or a neutrino, with branching fractions beta and 1 - beta, respectively. The search targets the decay final states comprising two electrons, or one electron and large missing transverse momentum, along with two quarks that are detected as hadronic jets. First-generation scalar leptoquarks with masses below 1435 (1270) GeVare excluded for beta = 1.0(0.5). These are the most stringent limits on the mass of first-generation scalar leptoquarks to date. The data are also interpreted to set exclusion limits in the context of an R-parity violating supersymmetric model, predicting promptly decaying top squarks with a similar dielectron final state.

PHYSICAL REVIEW D [99], 5, 052002, 2019. DOI: 10.1103/PhysRevD.99.052002

[P213-2019] "Search for resonant production of second-generation sleptons with same-sign dimuon events in proton--proton collisions at root s=13 TeV"

Sirunyan, A. M.; Tumasyan, A.; Adam, W.; **Chinellato, J. A.*; Tonelli Manganote, E. J.***; et. al.; CMS Collaboration

A search is presented for resonant production of second-generation sleptons ((mu) over tilde (L),(nu) over tilde (mu)) via the R-parityviolating coupling. gimel'(211) to quarks, in events with two samesign muons and at least two jets in the final state. The smuon (muon sneutrino) is expected to decay into amuon and a neutralino (chargino), which will then decay into a second muon and at least two jets. The analysis is based on the 2016 data set of proton- proton collisions at root s = 13 TeV recorded with the CMS detector at the LHC, corresponding to an integrated luminosity of 35.9 fb(-1).

No significant deviation is observed with respect to standard model expectations. Upper limits on cross sections, ranging from 0.24 to 730 fb, are derived in the context of two simplified models representing the dominant signal contributions leading to a same- sign muon pair. The cross section limits are translated into coupling limits for a modified constrained minimal supersymmetric model with. gimel'(211) as the only nonzero R-parity violating coupling. The results significantly extend restrictions of the parameter space compared with previous searches for similar models.

EUROPEAN PHYSICAL JOURNAL C [79], 4, 305, 2019. DOI: 10.1140/epjc/s10052-019-6800-x

[P214-2019] "Search for resonant t(t)over-bar production in proton-proton collisions at root s=13 TeV"

Sirunyan, A. M.; Tumasyan, A.; Adam, W.; **Chinellato, J. A.*; Tonelli Manganote, E. J.***; et. al.; CMS Collaboration

A search for a heavy resonance decaying into a top quark and antiquark (tt) pair is performed using proton-proton collisions at p s = 13TeV. The search uses the data set collected with the CMS detector in 2016, which corresponds to an integrated luminosity of 35.9 fb. The analysis considers three exclusive fi nal states and uses reconstruction techniques that are optimized for top quarks with high Lorentz boosts, which requires the use of nonisolated leptons and jet substructure techniques. No signi fi cant excess of events relative to the expected yield from standard model processes is observed. Upper limits on the production cross section of heavy resonances decaying to a tt pair are calculated. Limits are derived for a leptophobic topcolor Z 0 resonance with widths of 1, 10, and 30%, relative to the mass of the resonance, and exclude masses up to 3.80, 5.25, and 6.65TeV, respectively. Kaluza-Klein excitations of the gluon in the Randall-Sundrum model are excluded up to 4.55TeV. To date, these are the most stringent limits on tt resonances.

JOURNAL OF HIGH ENERGY PHYSICS [4], 031, 2019. DOI: 10.1007/JHEP04(2019)031

[P215-2019] "Search for the pair production of light top squarks in the e(+/-)mu(-/+) final state in proton-proton collisions at root s=13 TeV"

Sirunyan, A. M.; Tumasyan, A.; Adam, W.; **Chinellato, J. A.*; Tonelli Manganote, E. J.***; et. al.; CMS Collaboration

A search for the production of a pair of top squarks at the LHC is presented. This search targets a region of parameter space where the kinematics of top squark pair production and top quark pair production are very similar, because of the mass difference between the top squark and the neutralino being close to the top quark mass. The search is performed with 35.9 fb(-1) of proton-proton collisions at a centre-of-mass energy of root s = 13 TeV, collected by the CMS detector in 2016, using events containing one electron-muon pair with opposite charge. The search is based on a precise estimate of the top quark pair background, and the use of the M-T2 variable, which combines the transverse mass of each lepton and the missing transverse momentum. No excess of events is found over the standard model predictions. Exclusion limits are placed at 95% confidence level on the production of top squarks up to masses of 208 GeV for models with a mass difference between the top squark and the lightest neutralino close to that of the top quark.

JOURNAL OF HIGH ENERGY PHYSICS [3], 101, 2019. DOI: 10.1007/JHEP03(2019)101

[P216-2019] "Search for top quark partners with charge 5/3 in the same-sign dilepton and single-lepton final states in proton-proton collisions at root s=13 TeV"

Sirunyan, A. M.; Tumasyan, A.; Adam, W.; **Chinellato, J. A.*; Tonelli Manganote, E. J.***; et. al.; CMS Collaboration

A search for the pair production of heavy fermionic partners of the top quark with charge 5/3 (X-5/3) is performed in proton-proton collisions at a center-of-mass energy of 13 TeV with the CMS detector at the CERN LHC. The data sample analyzed corresponds to an integrated luminosity of 35.9 fb(-1). The X-5/3 quark is assumed always to decay into a top quark and a W boson. Both the right-handed and left--handed X-5/3 couplings to the W boson are considered. Final states with either a pair of same-sign leptons or a single lepton are studied. No significant excess of events is observed above the expected standard model background. Lower limits at 95% confidence level on the X-5/3 quark mass are set at 1.33 and 1.30 TeV respectively for the case of right--handed and left-handed couplings to W bosons in a combination of the same-sign dilepton and single-lepton final states.

JOURNAL OF HIGH ENERGY PHYSICS [3], 082, 2019. DOI: 10.1007/JHEP03(2019)082

[P217-2019] "Search for vector-like quarks in events with two oppositely charged leptons and jets in proton-proton collisions at root s=13TeV"

Sirunyan, A. M.; Tumasyan, A.; Adam, W.; **Chinellato, J. A.*; Tonelli Manganote, E. J.***; et. al. ; CMS Collaboration

A search for the pair production of heavy vector-like partners T and B of the top and bottom quarks has been performed by the CMS experiment at the CERN LHC using proton-proton collisions at . The data sample was collected in 2016 and corresponds to an integrated luminosity of 35.9 production include those where one of the T quarks decays via TtZ and the other via TbW, tZ, or tH, where H is a Higgs boson. For the BB case, final states include those where one of the B quarks decays via BbZ and the other BtW, bZ, or bH. Events with two oppositely charged electrons or muons, consistent with coming from the decay of a Z boson, and jets are investigated. The number of observed events is consistent with standard model background estimations. Lower limits at 95% confidence level are placed on the masses of the T and B quarks for a range of branching fractions. Assuming 100% branching fractions for TtZ, and BbZ, T and B quark mass values below 1280 and 1130 respectively, are excluded.

EUROPEAN PHYSICAL JOURNAL C [79], 4, 364, 2019. DOI: 10.1140/epjc/s10052-019-6855-8

[P218-2019] "Search for W Boson Decays to Three Charged Pions"

Sirunyan, A. M.; Tumasyan, A.; Adam, W.; **Chinellato, J. A.*; Tonelli Manganote, E. J.***; et. al.; CMS Collaboration

For the first time, a search for the rare decay of the W boson to three charged pions has been performed. Proton-proton collision data recorded by the CMS experiment at a center-of-mass energy of 13 TeV, corresponding to an integrated luminosity of 77.3 fb(-1), have been analyzed. No significant excess is observed above the background expectation. An upper limit of 1.01 x 10(-6) is set at 95% confidence level on the branching fraction of the W boson to three charged pions. This provides a strong motivation for theoretical calculations of this branching fraction.

PHYSICAL REVIEW LETTERS [122], 15, 151802, 2019. DOI: 10.1103/PhysRevLett.122.151802

[P219-2019] "Self-Calibrated Double Luminescent Thermometers Through Upconverting Nanoparticles"

Brites, C. D. S.; **Martinez, E. D.*; Urbano, R. R.*; Rettori, C.***; Carlos, L. D.

Luminescent nanothermometry uses the light emission from nanostructures for temperature measuring. Non-contact temperature readout opens new possibilities of tracking thermal flows at the sub-micrometer spatial scale, that are altering our understanding of heat-transfer phenomena occurring at living cells, micro electromagnetic machines or integrated electronic circuits, bringing also challenges of calibrating the luminescent nanoparticles for covering diverse temperature ranges. In this work, we report self-calibrated double luminescent thermometers, embedding in a poly(methyl methacrylate) film Er3+- -and Tm3+-doped upconverting nanoparticles. The Er3+-based primary thermometer uses the ratio between the integrated intensities of the H-2(11/2) -> I-4(15/2) and S-4(3/2) -> I-4(15/2) transitions (that follows the Boltzmann equation) to determine the temperature. It is used to calibrate the Tm3+/Er3+ secondary thermometer, which is based on the ratio between the integrated intensities of the (1)G(4) -> H-3(6) (Tm3+) and the S-4(3/2) -> I-4(15/2) (Er3+) transitions, displaying a maximum relative sensitivity of 2.96% K-1 and a minimum temperature uncertainty of 0.07 K. As the Tm3+/Er3+ ratio is calibrated trough the primary thermometer it avoids recurrent calibration procedures whenever the system operates in new experimental conditions.

FRONTIERS IN CHEMISTRY [7], 267, 2019. DOI: 10.3389/fchem.2019.00267

[P220-2019] "Signatures of Microevolutionary Processes in Phylogenetic Patterns"

Costa, C. L. N.; **Lemos-Costa, P.*; Marquitti, F. M. D.***; Fernandes, L. D.; **Ramos, M. F.*; Schneider, D. M.*; Martins, A. B.*; de Aguiar, M. A. M.***

Phylogenetic trees are representations of evolutionary relationships among species and contain signatures of the processes responsible for the speciation events they display. Inferring processes from tree properties, however, is challenging. To address this problem, we analyzed a spatially-explicit model of speciation where genome size and mating range can be controlled. We simulated parapatric and sympatric (narrow and wide mating range, respectively) radiations and constructed their phylogenetic trees, computing structural properties such as tree balance and speed of diversification. We showed that parapatric and sympatric speciation are well separated by these structural tree properties. Balanced trees with constant rates of diversification only originate in sympatry and genome size affected both the balance and the speed of diversification of the simulated trees. Comparison with empirical data showed that most of the evolutionary radiations considered to have developed in parapatry or sympatry are in good agreement with model predictions. Even though additional forces other than spatial restriction of gene flow, genome size, and genetic incompatibilities, do play a role in the evolution of species formation, the microevolutionary processes modeled here capture signatures of the diversification pattern of evolutionary radiations, regarding the symmetry and speed of diversification of lineages.

SYSTEMATIC BIOLOGY [68], 1, 131-144, 2019. DOI: 10.1093/sysbio/syy049

[P221-2019] "Silver nanoparticles produced by laser ablation for a study on the effect of SERS with low laser power on N719 dye and Rhodamine-B"

Borrero, N. F. V.*; Silva Filho, J. M. C.*; Ermakov, V. A.*; Marques, F. C.*

The effect of surface-enhanced Raman spectroscopy (SERS) was investigated in N719 dye thin films deposited on silicon wafer with a thin film of silver nanoparticles (Ag-NPs) fabricated by laser ablation in an aqueous solution, using a NdYAG laser (lambda = 1064nm). Optical absorption spectroscopy of the Ag-NPs colloidal solution shows an absorption peak at lambda = 400nm, associated with a localized surface plasmon resonance in the Ag-Isff's. Scanning electron microscopy (SEM) reveals that these NPs have an approximately spherical shape, with their diameter being tunable by laser power intensity. Raman spectroscopy measurements were performed using low laser power to avoid damage to the N719 dye films. Thus, a small Raman signal is obtained. The Raman intensity was greatly increased when the N719 film was deposited on a substrate with a thin film of Ag-NPs due to the SERS effect. The process was also used in Rhodamine-B to clearly demonstrate the SERS effect obtained by the use of these NPs produced by laser ablation.

MRS ADVANCES [4], 11-12, 723-731, 2019. DOI: 10.1557/adv.2019.157

[P222-2019] "Statistical Mesoscopic Hydro-thermodynamics: the Description of Kinetics and Hydrodynamics of Nonequilibrium Processes in Single Liquids"

Ramos, J. G.*; Rodrigues, C. G.; Silva, C. A. B.; **Luzzi, R.***

Hydrodynamics, a term apparently introduced by Daniel Bernoulli (1700-1783) to comprise hydrostatic and hydraulics, has a long history with several theoretical approaches. Here, after a descriptive introduction, we present so-called mesoscopic hydro-thermodynamics, which is also referred to as higher order generalized hydrodynamics, built within the framework of a mechanical-statistical formalism. It consists of a description of the material and heat motion of fluids in terms of the corresponding densities and their associated fluxes of all orders. In this way, movements are characterized in terms of intermediate to short wavelengths and intermediate to high frequencies. The fluxes have associated Maxwell-like times, which play an important role in determining the appropriate contraction of the description (of the enormous set of fluxes of all orders) necessary to address the characterization of the motion in each experimental setup. This study is an extension of a preliminary article: Physical Review E 91, 063011 (2015).

BRAZILIAN JOURNAL OF PHYSICS [49], 2, 277-287, 2019. DOI: 10.1007/s13538-019-00639-8

[P223-2019] "Steve: A Hierarchical Bayesian Model for Supernova Cosmology"

Hinton, S. R.; Davis, T. M.; Kim, A. G.; **Sobreira, F.***; et. al.

We present a new Bayesian hierarchical model (BHM) named Steve for performing Type Ia supernova (SN Ia) cosmology fits. This advances previous works by including an improved treatment of Malmquist bias, accounting for additional sources of systematic uncertainty, and increasing numerical efficiency. Given light-curve fit parameters, redshifts, and host-galaxy masses, we fit Steve simultaneously for parameters describing cosmology, SN Ia populations, and systematic uncertainties. Selection effects are characterized using Monte Carlo simulations. We demonstrate its implementation by fitting realizations of SN Ia data sets where the SN Ia model closely follows that used in Steve. Next, we validate on more realistic SNANA simulations of SN Ia samples from the Dark Energy Survey and low--redshift surveys (DES Collaboration et al. 2018). These simulated data sets contain more than 60,000 SNe Ia, which we use to evaluate biases in the recovery of cosmological parameters, specifically the equation of state of dark energy, w. This is the most rigorous test of a BHM method applied to SN Ia cosmology fitting and reveals small w biases that depend on the simulated SN Ia properties, in particular the intrinsic SN Ia scatter model.

This w bias is less than 0.03 on average, less than half the statistical uncertainty on w. These simulation test results are a concern for BHM cosmology fitting applications on large upcoming surveys; therefore, future development will focus on minimizing the sensitivity of Steve to the SN Ia intrinsic scatter model.

ASTROPHYSICAL JOURNAL [876], 1, 15, 2019. DOI: 10.3847/1538-4357/ab13a3

[P224-2019] "Stimulated electron energy loss and gain in an electron microscope without a pulsed electron gun"

Das, P.; Blazit, J. D.; Tence, M.; **Zagonel, L. F.*; Auad, Y.***; Lee, Y. H.; Ling, X. Y.; Losquin, A.; Colliex, C.; Stephan, O.; Garcia de Abajo, F. J.; Kociak, M.

We report on a novel way of performing stimulated electron energy-loss and energy-gain spectroscopy (sEELS/sEEGS) experiments that does not require a pulsed gun. In this scheme, a regular scanning transmission electron microscope (STEM) equipped with a conventional continuous electron gun is fitted with a modified EELS detector and a light injector in the object chamber. The modification of the EELS detector allows one to expose the EELS camera during tunable time intervals that can be synchronized with nanosecond laser pulses hitting the sample, therefore allowing us to collect only those electrons that have interacted with the sample under light irradiation. Using similar to 5 ns laser pulses of similar to 2 eV photon energy on various plasmonic silver samples, we obtain evidence of sEELS/sEEGS through the emergence of up to two loss and gain peaks in the spectra at +/- 2 and +/- 4 eV. Because this approach does not involve any modification of the gun, our method retains the original performances of the microscope in terms of energy resolution and spectral imaging with and without light injection. Compared to pulsed-gun techniques, our method is mainly limited to a perturbative regime (typically no more that one gain event per incident electron), which allows us to observe resonant effects, in particular when the plasmon energy of a silver nanostructure matches the laser photon energy. In this situation, EELS and EEGS signals are enhanced in proportion to n + 1 and n, respectively, where n is the average plasmon population due to the external illumination. The n term is associated with stimulated loss and gain processes, and the term of 1 corresponds to conventional (spontaneous) loss. The EELS part of the spectrum is therefore an incoherent superposition of spontaneous and stimulated EEL events. This is confirmed by a proper quantum-mechanical description of the electron/light/plasmon system incorporating light-plasmon and plasmon-electron interactions, as well as inelastic plasmon decay.

ULTRAMICROSCOPY [203], SI, 44-51, 2019. DOI: 10.1016/j.ultramic.2018.12.011

[P225-2019] "Substrate Bias Voltage Tailoring the Interfacial Chemistry of a-SiCx:H: A Surprising Improvement in Adhesion of a-C:H Thin Films Deposited on Ferrous Alloys Controlled by Oxygen"

Crespi, A. E.; Leidens, L. M.; **Antunes, V.***; Perotti, B. L.; Michels, A. F.; **Alvarez, F.***; Figueroa, C. A.

Hydrogenated amorphous carbon thin films (a-C:H) have attracted much attention because of their surprising properties, including ultralow friction coefficients in specific conditions. Adhesion of a-C:H films on ferrous alloys is poor due to chemical and physical aspects, avoiding a widespread application of such a film. One possibility to overcome this drawback is depositing an interlayer-an intermediate thin film-between the carbon-based coating and the substrate to improve chemical interaction and adhesion. Based on this, interlayers play a key role on a-C:H thin-film adhesion through a better chemical network structure at the outermost layer of the a-SiCx:H interlayer, i.e., the a-C:H/a--SiCx:H interface. However, despite the latest important advances on the subject, the coating adhesion continues being a cumbersome problem since it depends on multifactorial causes. Thus, the purpose of this paper is to report a standard protocol leading to surprising good results based on the control of the interfacial chemical bonding by properly biasing the substrate (between 500 and 800 V) during the a-SiCx:H interlayer deposition at an appropriate low temperature, by using hexamethyldisiloxane as precursor. The interlayers and the outermost interfaces were analyzed by a comprehensive set of techniques, including X-ray photoelectron spectroscopy, glow discharge optical emission spectroscopy, and Fourier transform infrared spectroscopy. Nanoscratch tests, complemented by scanning electron microscopy and energy-dispersive X-ray spectroscopy, were used to evaluate the critical load for delamination to certify and quantify the adhesion improvement. This study was important to identify the chemical local bonding of the elements at the interface and its local environment, including the in-depth chemical composition profile of the coating. An important effect is that the oxygen content decreases on increasing substrate bias voltage, improving the adhesion of the film. This is due to the fact that energetic ion hitting the growing interlayer breaks Si-O and C-O bonds, augmenting the content of Si-C and C-C bonds at the outermost interface of the a-SiCx:H interlayer and enhancing the a--C:H coating adhesion. Moreover, the combination of high bias voltage (800 V) and low temperature (150 degrees C) during the a-SiCx:H interlayer deposition allows good adhesion of a--C:H thin films due to sputtering of light elements like oxygen. Therefore, an appropriated bias and temperature combination can open new pathways in a-C:H thin-film deposition at low temperatures. These results are particularly interesting for temperature-sensible metal alloys, where well adhered a-C:H thin films are mandatory for tribological applications.

ACS APPLIED MATERIALS & INTERFACES [11], 19, 18024-18033, 2019. DOI: 10.1021/acsami.9b03597

[P226-2019] "Surface structure characterization by X-ray photoelectron diffraction of Sn ultra-thin films deposited on Pd(111)"

Pancotti, A.; **de Siervo, A.***; Carazzolle, M. F.; Silva, J. J.; Nascente, P. A. P.; **Landers, R.***

The formation of surface alloys obtained by annealing ultra--thin films of Sn deposited on a Pd(111) surface was characterized by X-ray photoelectron spectroscopy (XPS), low--energy electron diffraction (LEED), and X-ray photoelectron diffraction (XPD). Annealing the surface at 600 K produced a (root 3x root 3)R30 degrees LEED pattern, and the comparison between experimental and theoretical XPD results indicated the formation of a corrugated bi-dimensional Pd2Sn surface alloy, with Sn atoms being present not only on the outmost layer but also at least on the second internal layer.

SURFACE SCIENCE [685], 7-12, 2019. DOI: 10.1016/j.susc.2019.01.014

[P227-2019] "The dark matter puzzle in a class of models with gauge symmetry SU(3)(C) circle times SU(3)(L) circle times U(1)(N)"

Alvarez-Salazar, C. E.*; Peres, O. L. G.*; Sanchez-Vega, B. L.

We analyze the dark matter (DM) puzzle in a class of models with gauge symmetry SU(3)(C) circle times SU(3)(L) circle times U(1)(N),

taking into account the constraints coming from Planck observations of the DM relic density, direct detection searches with Xenon1T, and indirect detection using Fermi-LAT data. The model has two possible candidates, a fermion and a scalar, which require, to evade the constraints set by Xenon1T and Fermi-LAT, and have relic densities in the range measured by the Planck collaboration, a minimum vacuum expectation value to break the SU(3)(L)symmetry of 10 and 15 TeV, respectively. In this case, these particles have masses of order 1 TeV, for the fermion, and between 500 and 600 GeV, for the scalar.

ASTRONOMISCHE NACHRICHTEN [340], 1-3, SI, 135-138, 2019. DOI: 10.1002/asna.201913577

[P228-2019] "The linear Dirac spectrum and the Weyl states in the Drude-Sommerfeld topological model"

Doria, M. M.*

Weyl fermions are shown to exist in a Drude-Sommerfeld topological model (DSTM), that features nearly free carriers in topological protected states under residual collisions. The Weyl fermion features a weak magnetic field around it, produced by its own currents, that dresses it, and is the key to its topological stability. The Weyl fermion state results from a Schroedinger like hamiltonian for particles with spin and magnetic energy which are momentum confined to a layer [M.M. Doria, A. Perali, Europhys. Lett. 119, 21001 (2017)]. The present mechanism for the onset of Weyl fermion breaks the reflection and time symmetries around the layer and displays an energy gap. Much above this gap the spectrum becomes linear (Dirac) and then momentum and spin become orthogonal (zero helicity state, ZHS). The collision time is shown to be renormalized by the inverse of the square of the gap in the linear Dirac spectrum limit. Hence the Weyl fermions are shown to be intrinsically ballistic in this limit. The Weyl fermion own magnetic field, although very weak, cannot be discarded because it yields a non zero Chern-Simons number, which is here calculated in the Dirac limit. The electrical and the thermal conductivities of the Weyl fermions are derived in the framework of a constant relaxation time. The Lorenz number coefficient associated to the Wiedemman-Franz law acquires asymptotic value of 6.5552 times the bulk value of pi(2)/3.

EUROPEAN PHYSICAL JOURNAL B [92], 3, 64, 2019. DOI: 10.1140/epjb/e2019-90591-2

[P229-2019] "Transfer learning for galaxy morphology from one survey to another"

Sanchez, H. D.; Huertas-Company, M.; Bernardi, M.; **Sobreira, F.***; et. al.

Deep learning (DL) algorithms for morphological classification of galaxies have proven very successful, mimicking (or even improving) visual classifications. However, these algorithms rely on large training samples of labelled galaxies (typically thousands of them). A key question for using DL classifications in future Big Data surveys is how much of the knowledge acquired from an existing survey can be exported to a new data set, i.e. if the features learned by the machines are meaningful for different data. We test the performance of DL models, trained with Sloan Digital Sky Survey (SDSS) data, on Dark Energy Survey (DES) using images for a sample of similar to 5000 galaxies with a similar redshift distribution to SDSS. Applying the models directly to DES data provides a reasonable global accuracy (similar to 90 per cent), but small completeness and purity values. A fast domain adaptation step, consisting of a further training with a small DES sample of galaxies (similar to 500-300), is enough for obtaining an accuracy >95 per cent and a significant improvement in the completeness and purity values. This demonstrates that, once trained with a particular data set, machines can quickly adapt to new instrument characteristics (e.g. PSF, seeing, depth), reducing by almost one order of magnitude the necessary training sample for morphological classification. Redshift evolution effects or significant depth differences are not taken into account in this study.

MONTHLY NOTICES OF THE ROYAL ASTRONOMICAL SOCIETY [484], 1, 93-100, 2019. DOI: 10.1093/mnras/sty3497

[P230-2019] "Vacuum stability conditions of the economical 3-3-1 model from copositivity"

Sanchez-Vega, B. L.; **Gambini, G.*; Alvarez-Salazar, C. E.***

By applying copositivity criterion to the scalar potential of the economical 3-3-1 model, we derive necessary and sufficient bounded-from-below conditions at tree level. Although these are a large number of intricate inequalities for the dimensionless parameters of the scalar potential, we present general enlightening relations in this work. Additionally, we use constraints coming from the minimization of the scalar potential by means of the orbit space method, the positivity of the squared masses of the extra scalars, the Higgs boson mass, the Z gauge boson mass and its mixing angle with the SM Z boson in order to further restrict the parameter space of this model.

EUROPEAN PHYSICAL JOURNAL C [79], 4, 299, 2019. DOI: 10.1140/epjc/s10052-019-6807-3

[P231-2019] "Weak-lensing analysis of SPT-selected galaxy clusters using Dark Energy Survey Science Verification data"

Stern, C.; Dietrich, J. P.; Bocquet, S.; **Sobreira, F.***; et. al.; DES Collaborations; SPT Collaborations

We present weak-lensing (WL) mass constraints for a sample of massive galaxy clusters detected by the South Pole Telescope (SPT) via the Sunyaev-Zel'dovich effect (SZE). We use griz imaging data obtained from the Science Verification (SV) phase of the Dark Energy Survey (DES) to fit the WL shear signal of 33 clusters in the redshift range 0.25 <= z <= 0.8 with NFW profiles and to constrain a four-parameter SPT mass-observable relation. To account for biases in WL masses, we introduce a WL mass to true mass scaling relation described by a mean bias and an intrinsic, lognormal scatter. We allow for correlated scatter within the WL and SZE mass-observable relations and use simulations to constrain priors on nuisance parameters related to bias and scatter from WL. We constrain the normalization of the zeta-M-500 relation, A(SZ) = 12.0(-6.7)(+2.6) when using a prior on the mass slope B-SZ from the latest SPT cluster cosmology analysis. Without this prior, we recover A(SZ) = 10.8(-5.2)(+2.3) and B-SZ = 1.30(-0.44)(+0.22). Results in both cases imply lower cluster masses than measured in previous work with and without WL, although the uncertainties are large. The WL derived value of B-SZ is approximate to 20 per cent lower than the value preferred by the most recent SPT cluster cosmology analysis. The method demonstrated in this work is designed to constrain cluster masses and cosmological parameters simultaneously and will form the basis for subsequent studies that employ the full SPT cluster sample together with the DES data.

MONTHLY NOTICES OF THE ROYAL ASTRONOMICAL SOCIETY [485], 1, 69-87, 2019. DOI: 10.1093/mnras/stz234

Correções

[Co001-2019] "Search for a new scalar resonance decaying to a pair of Z bosons in proton-proton collisions at root s = 13 TeV (vol 6, 127, 2018)"

Sirunyan, A. M.; Tumasyan, A.; Adam, W.; **Chinellato, J. A.*; Tonelli Manganote, E. J.***; et. al.; CMS Collaboration

In both panels of figure 11, the unit of the z axis was mistakenly written as pb when it should have been fb. The corrected versions are shown in figure 1.

JOURNAL OF HIGH ENERGY PHYSICS [3], 128, 2019. DOI: 10.1007/JHEP03(2019)128

***Autores da comunidade IFGW**
Fonte: Web of Science on-line (WOS)

Defesas de Teses do IFGW

[T006-2019] "Propriedades Estruturais, Ópticas e Mecânicas de Filmes Finos de Triiodeto de Bismuto (BiI3) Depositados por Evaporação Térmica"
Aluno: Natália de Faria Coutinho
Orientador: Prof. Dr. Francisco das Chagas Marques**Data: 03/07/2019**

Defesas de Dissertações do IFGW

[D005-2019] "Estudo do efeito da contaminação na luz de cintilação do argônio líquido no experimento ProtoDUNE-SP"
Aluno: Marina Reggiani Guzzo
Orientador: Prof. Dr. Ettore Segreto
Data: 10/06/2019

[D006-2019] "Neutrinos em um Modelo SU(3)xU(1) Mínimo"
Aluno: Sany Willian Ponce Novelo
Orientador: Prof. Dr. Marcelo Moraes Guzzo
Data: 19/06/2019

[D007-2019] "Modos quasinormais e estabilidade de um wormhole minimal"
Aluno: Laura Borges dos Penedos
Orientador: Prof. Dr. Alberto Vazquez Saa
Data: 19/06/2019

[D008-2019] "Transições de fase nos modelos do votante e do Moran em redes estruturadas"
Aluno: Gabriella Dantas Franco
Orientador: Prof. Dr. Marcus Aloizio Martinez de Aguiar
Data: 24/06/2019

[D009-2019] "Implicações Cosmológicas da Radiação Hawking do Horizonte de de Sitter"
Aluno: Juliano Choi Rodrigues
Orientador: Prof. Dr. Donato Giorgio Torrieri
Data: 26/06/2019

[D010-2019] "Caracterização de Wavelengh Shifters e otimização do dispositivo ARAPUCA"
Aluno: Bruno Passarelli Gelli
Orientador: Prof. Dr. Ettore Segreto
Data: 28/06/2019

[D011-2019] "Análise da oxigenação do tecido biológico durante um exercício de força"
Aluno: Giovani Grisotti Martins
Orientador: Prof. Dr. Rickson Coelho Mesquita
Data: 28/06/2019

[D012-2019] "Redistribuição de Correlações devido a Horizontes Causais"
Aluno: Leonardo Pipolo de Gioia
Orientador: Prof. Dr. Marcos César de Oliveira
Data: 28/06/2019

[D013-2019] "Investigação da técnica de neurofeedback utilizando fMRI, EEG e NIRS"
Aluno: Lucas Toffoli de Menezes
Orientador: Profa. Dra. Gabriela Castellano
Data: 28/06/2019

[D014-2019] "Procura por assinaturas de alinhamento induzido por campo magnético nas direções de chegada de raios cósmicos detectados no Observatório Pierre Auger"
Aluno: Rafael Geurgas Zavarizz
Orientador: Profa. Dra. Carola Dobrigkeit Chinellato
Data: 07/07/2019

Fonte: Portal IFGW/Pós-graduação - Agenda de Colóquios, Defesas e Seminários.
Disponível em: http://portal.ifi.unicamp.br/pos-graduacao

***Nestes meses não há Defesas de Dissertações e Teses do PECIM com Orientadores do IFGW.**

Abstracta

Instituto de Física
Diretor: Prof. Dr. Pascoal José Giglio Pagliuso
Diretora Associada: Profa. Dra. Mônica Alonso Cotta
Universidade Estadual de Campinas - UNICAMP
Cidade Universitária Zeferino Vaz
13083-859 - Campinas - SP - Brasil
e-mail: secdir@ifi.unicamp.br
Fone: +55 19 3521-5300

Publicação

Biblioteca do Instituto de Física Gleb Wataghin
http://portal.ifi.unicamp.br/biblioteca

Diretora Técnica: Sandra Maria Carlos Cartaxo
Coordenadora da Comissão de Biblioteca: Profa. Dra. Arlene Cristina Aguilar

Elaboração:
Maria Graciele Trevisan (Bibliotecária)
Ayres Neri da Cunha Junior (Técnico Administrativo)
contato: infobif@ifi.unicamp.br